JOURNAL OF GUIDANCE, CONTROL, AND DYNAMICS
Vol. 32, No. 1, January–February 2009

Integrated Higher-Order Sliding Mode Guidance and Autopilot for Dual-Control Missiles

Yuri B. Shtessel*
University of Alabama in Huntsville, Huntsville, Alabama 35899
and
Christian H. Tournes†
Davidson Technologies, Inc., Huntsville, Alabama 35805

DOI: 10.2514/1.36961

An integrated autopilot and guidance algorithm, robust to target maneuvers and missile's model uncertainties, is developed using higher-order sliding mode control for interceptors steered by a combination of aerodynamic lift, sustainer thrust, and center-of-gravity divert thrusters. A smooth higher-order sliding mode guidance that is robust to target maneuvers generates flight-path trajectory angular rates and attitude rate commands. The attitude rate missile maneuvers are aimed at producing desired aerodynamic lift and/or orienting the sustainer thrust. The lateral acceleration created by the missile attitude maneuver is treated as a cooperative disturbance and accounted for by the trajectory control. Robust to the missile's model uncertainties, higher-order (second-order) sliding mode autopilot is designed based on a nonlinear dynamic sliding manifold. The proposed integrated autopilot and guidance algorithm also includes seeker/tracker bore-sight stabilization and estimation of target lateral acceleration. The algorithm is tested using computer simulations against a ballistic maneuvering target.

Nomenclature

a_α, a_δ, a_Δ	=	distance from the center of gravity along the longitudinal axis of the aerodynamic center and application points of attitude and divert thrusters, m
C_{L_α}	=	lift-coefficient gradient with respect to angle of attack α
C_{L_q}	=	lift-coefficient gradient with respect to angle of attack q
$\bar{C}$	=	reference length, m
D_α, D_δ, D_Δ	=	disturbance terms that are uniformly distributed within $\pm D$ intervals
d_α	=	disturbance factor applied to aerodynamic lift
d_Δ	=	disturbance factor applied to divert thrusters
d_δ	=	disturbance factor applied to attitude thrusters
f_q, f_γ, f_α	=	additive disturbances
g	=	acceleration of Earth's gravity, $\mathrm{m/s^2}$
I_{yy}	=	moment of inertia around the pitch axis, $\mathrm{kg \cdot m^2}$
M_α	=	pitch-rate stability derivative with respect to α, $\mathrm{s^{-2}}$
M_Δ	=	pitch-rate stability derivative with respect to Δ, $\mathrm{s^{-2}}$
M_δ	=	pitch-rate stability derivative with respect to δ, $\mathrm{s^{-2}}$
M_ζ	=	pitch-rate stability derivative with respect to ς, $\mathrm{s^{-2}}$
m	=	missile mass, kg
q	=	pitch rate, rad/s
r	=	target-interceptor range along line of sight, m
T_Δ	=	divert thrust, N
T_δ	=	attitude thrust, N
T_ζ	=	sustainer thrust, N
$T_{\max\delta}$, $T_{\max\Delta}$	=	maximum sustainer attitude and divert thrust, N
u_Δ	=	divert thruster commands
u_δ	=	attitude commands
u_ζ	=	thrust vector control normalized commands
V	=	longitudinal velocity of a missile, m/s
$V_\parallel$	=	relative velocity component parallel to line of site, m/s
$V_\perp$	=	relative velocity component normal to line of site, m/s
Z	=	trajectory stability derivative with respect to q, $\mathrm{s^{-1}}$
Z_α	=	trajectory stability derivative with respect to α, $\mathrm{s^{-1}}$
Z_Δ	=	trajectory stability derivative with respect to Δ, $\mathrm{s^{-1}}$
Z_δ	=	trajectory stability derivative with respect to δ, $\mathrm{s^{-1}}$
Z_ζ	=	trajectory stability derivative with respect to ς, $\mathrm{s^{-1}}$
α	=	angle of attack, rad
Γ	=	actual-interceptor normal acceleration, $\mathrm{m/s^2}$
$\Gamma_{\max}$	=	maximum-interceptor normal acceleration, $\mathrm{m/s^2}$
$\hat{\Gamma}_\mathbf{T}$	=	estimated target acceleration vector, $\mathrm{m/s^2}$
$\Gamma_\parallel$	=	target acceleration component along line of sight, $\mathrm{m/s^2}$
$\Gamma_\perp$	=	target acceleration component normal to the line of sight, $\mathrm{m/s^2}$
Γ^*	=	commanded-interceptor normal acceleration, $\mathrm{m/s^2}$
γ	=	flight-path angles, rad
Δ	=	divert-thruster forces
δ	=	normalized attitude forces
δ_ε	=	disturbance factor applied to seeker measurement noise
ε_α	=	angle-of-attack tracking errors
ε_γ	=	flight-path angle tracking errors. rad
ε_q	=	pitch-rate tracking errors, rad/s

Presented as Paper 6784 at the AIAA Guidance, Navigation, and Control Conference and Exhibit, Keystone, CO, August 21–24, 2006; received 2 February 2008; revision received 14 May 2008; accepted for publication 23 May 2008.

*Professor, Department of Electrical and Computer Engineering; Shtessel@ece.uah.edu. Associate Fellow AIAA.

†Chief Scientist; Adjunct Professor, The University of Alabama in Huntsville; ChristianTournes@Davidson-Tech.com. Senior Member AIAA.

ζ = thrust vectoring control, rad
λ = line-of-sight angle, rad
$\hat{\lambda}$ = bore-sight angle, rad
ρ = air specific mass, kg/m^3
τ_Δ = time constant of divert thrusters, s
τ_δ = time constant of attitude, s
τ_ζ = time constant of thrust vector control actuators, s
ω, ω', ω'', ω''' = characteristic frequencies of the seeker prefilter, guidance surface, seeker passband, and seeker platform dynamics, rad/s
ω_λ = rotation rate of the line of sight, rad/s
ϖ, ϖ', ϖ'', ϖ''' = characteristic frequencies of flight-path, pitch and angle-of-attack autopilots, and seeker surface, rad/s
$\_$ = filtered variable

Subscripts

δ, Δ = value, variable associated with attitude and divert thrusters

Superscripts

ε = angular and linear tracking error with respect to variable (.)
$*$ = commanded, reference value of variable (.)
$'$ = variable associated with seeker bore-sight steering
$''$ = variable associated with guidance

I. Introduction

THE evolution of advanced threats with their growing maneuvering capabilities calls for interceptors with increased maneuvering agility operating seamlessly in and between the boundaries of low endo-, high endo-, and exoatmospheric regimes. It also creates new challenges for missile defense interceptor designs, including the development of the robust and accurate guidance, navigation, and control laws and their integration.

To cope with increasingly larger target maneuvering capabilities, a future interceptor, as shown Fig. 1, may be steered by a possible combination of aerodynamic-lift, sustainer or last stage-thrust, and center-of-gravity (c.g.) divert thrusters. Attitude steering may be achieved by continuous actuators such as thrust vector control (TVC) as well as pulse-width modulated thrusters. This poses serious guidance, navigation, and control challenges. They include the following:

1) Anticipated targets may engage in combinations of quasi-random helical-type maneuvers and deterministic possibly powered maneuvers. This may include sine waved target lateral accelerations, as well as step maneuvers with sudden changes of polarity. It is crucial to design guidance laws requiring missile-to-target acceleration advantages as close to one as possible. Increasing interceptor divert capability could be achieved using combinations of divert modes such as aerodynamic lift and c.g. divert thrusters, which have essentially different dynamic responses [1]. The angle-of-attack maneuver affects the exhaust conditions of the thrusters; likewise thruster jets' operation affects the system of shock waves around the interceptor. This results in relative model uncertainties as large as 30% changing rapidly with the firing of the thrusters, thereby raising an extremely serious robustness issue [1]. In addition to laterally steering the interceptor with a combination of aerodynamic lift and a divert thruster, TVC is proposed, as shown Fig. 2 [2]. The autopilot must handle continuous actuators such as TVC as well as pulse-width modulated thrusters. The design of dual-concurrent-control systems is challenging because the two concurrent controls share the same output; that is, the actual interceptor acceleration.

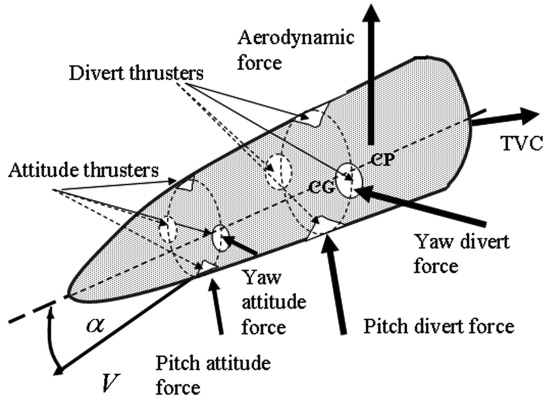

Fig. 2 Dual-thrust-controlled interceptor.

2) Controlling the angle-of-attack maneuvers to steer missile trajectory requires first calculating the command angle of attack/pitch rate, a process also referred to as *inversion*, and then track the tracking corresponding variables [3]; when conventional control techniques are used the inner-loop response must be faster than the response of the guidance (outer loop). Another problem is posed by the accuracy of the inversion due to model uncertainties. A possible solution to the inversion is the use of disturbance observers [4].

3) Target maneuvers render the target prediction problematic, in particular when it comes to estimating target acceleration. This is particularly critical with Kalman filters that converge asymptotically. The seeker does not measure the line of sight to the target but an angular error with respect to current seeker bore sight. Therefore, the seeker's dynamics must be compensated taking into account the measurement noise that is challenging [3,5].

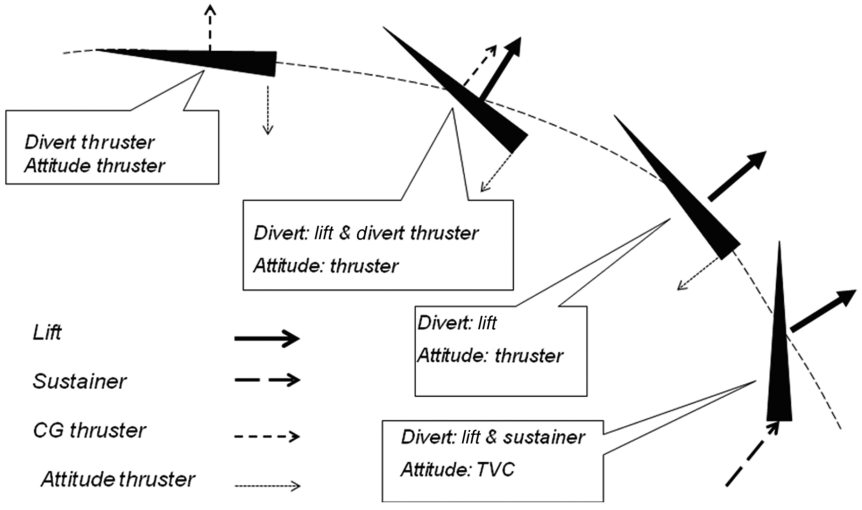

Fig. 1 Different modus operandi.

Addressing the outlined challenges, the goal of this work is in developing integrated robust sensor information processing and data estimation, a homing guidance law, and autopilot guidance and control technology for dual-controlled missile interceptors via higher-order (second-order) sliding mode (HOSM) control and observers to achieve the hit-to-kill accuracy against targets performing high-amplitude evasive maneuvers.

Integrated guidance and automatic pilot using traditional sliding mode control (SMC) [6] was studied in [7]. The integrated controller uses a canard control to steer a first sliding variable representing the zero effort miss (ZEM) to zero, and a second sliding variable representing pitch acceleration contributions of the angle of attack and tail control is also driven to zero. Traditional SMC is used for developing robust to target maneuvers guidance laws for missile interceptors [7–13]. The approximation of traditional SMC by saturation functions is employed [6] to smooth out the guidance command at a price of loosing robustness. HOSM/SOSM (second-order sliding mode control) [14–18] mitigates the problems associated with SMC; that is, HOSM is applicable to the systems with arbitrary relative degree, and continuous/smooth control functions can be designed, retaining the robustness. Development of the *smooth* robust guidance law to target maneuvers [15,16] is essential for effectively following this law by the autopilot and also for integrating guidance and autopilot [7,9,17].

In this work the robust to target maneuvers and autopilot uncertainties multiple-loop integrated guidance and autopilot is studied using entirely SOSM control techniques, for which basics are presented in the Appendix. Smooth second-order sliding mode (SSOSM) control techniques are used to orient the seeker bore sight (collapse of the seeker compensated dynamics is achieved) and to achieve a smooth estimation of target acceleration in finite time. The missile-interceptor SSOSM-based robust guidance law [15] is integrated into a dual-controlled SOSM-based missile autopilot [2,17] using an inversion to generate a smooth flight-path angle, angle-of-attack, and pitch-rate autopilot commands.

The use of aerodynamic lift increases the divert capability of the missile up to 100%, and the use of divert thrusters provides a fast response to the guidance command. Model uncertainties created by the interactions between the airflow and the thruster jets are taken into account and compensated for by SOSM-based autopilot. The integrated SOSM guidance–autopilot algorithm is tested via computer simulations against ballistic maneuvering targets.

II. Mathematical Model and Problem Formulation

The following state model [15,17] of missile-target engagement kinematics (Fig. 3) is used:

$$\begin{cases} \dot{r} = V_{\parallel} \\ \dot{V}_{\parallel} = -V_{\perp}^2/r + \Gamma_{\parallel} + \sin(\gamma - \lambda)\Gamma \\ \dot{\lambda} = V_{\perp}/r \\ \dot{V}_{\perp} = -V_{\parallel}V_{\perp}/r + \Gamma_{\perp} - \cos(\gamma - \lambda)\Gamma \end{cases} \tag{1}$$

where r is the range along the line of site (LOS); λ is the LOS angle; γ is a missile flight-path angle; $\dot{\lambda} = \omega_{\lambda}$ rad/s^2 is the LOS rate; $V_{\perp} = r\omega_{\lambda}$ m/s is a transversal component of relative velocity in the reference frame rotating with the LOS; Γ is missile normal acceleration; and $\Gamma_{\parallel}$ and $\Gamma_{\perp}$ m/s^2 (disturbances) are projections of bounded target acceleration along and orthogonal to the LOS. The dynamics of a missile steered by the combined effects of divert thrusters and the pitch maneuver are given by [2,17,19]

$$\dot{\alpha} = q - Z_{\alpha}(1 + \bar{d}_{\alpha})\alpha + \frac{g}{V}\cos(\gamma) - Z_{\delta}(1 + \bar{d}_{\delta})\cos(\alpha)\delta - Z_{\Delta}(1 + \bar{d}_{\Delta})\cos(\alpha)\Delta - \cos(\alpha)Z_{\varsigma}\varsigma \tag{2}$$

$$\dot{q} = M_{\alpha}(1 + \bar{d}_{\alpha})\alpha + M_q q + M_{\Delta}(1 + \bar{d}_{\Delta})\Delta + M_{\delta}(1 + \bar{d}_{\delta})\delta + M_{\varsigma}\varsigma \tag{3}$$

$$\dot{\gamma} = Z_{\alpha}(1 + \bar{d}_{\alpha})\alpha + Z_q q - \frac{g}{V}\cos(\gamma) + Z_{\delta}(1 + \bar{d}_{\delta})\cos(\alpha)\delta + Z_{\Delta}(1 + \bar{d}_{\Delta})\cos(\alpha)\Delta + \cos(\alpha)Z_{\varsigma}\varsigma \tag{4}$$

where

$$Z_{\alpha} = \frac{\rho S V C_{L_{\alpha}}}{2m}, \quad Z_{\delta} = \frac{T_{\max\delta}}{mV}, \quad Z_{\Delta} = \frac{T_{\max\Delta}}{mV}, \quad Z_q = \frac{\rho S\bar{C} C_{L_q}}{2m}$$

$$Z_{\zeta} = \frac{T_s}{mV}, \quad M_{\alpha} = \frac{\rho S\bar{C} V^2 C_{L_{\alpha}}}{2I_{yy}}, \quad M_q = \frac{\rho S\bar{C}^2 V C_{L_q}}{2I_{yy}}$$

$$M_{\delta} = \frac{a_{\delta}T_{\max\delta}}{I_{yy}}, \quad M_{\Delta} = \frac{a_{\Delta}T_{\max\Delta}}{I_{yy}}, \quad M_{\zeta} = \frac{a_s T_s}{I_{yy}}$$

and α, γ, and q represent the angle of attack, flight-path angles (rad), and pitch rate (rad/s), respectively; V is the longitudinal velocity of a missile (m/s). The cumulative disturbances $\bar{d}_{\alpha}$, $\bar{d}_{\delta}$, and $\bar{d}_{\Delta}$ represent the unknown interactions between attitude thruster jets, divert thruster jets, and shock waves as well as bounded slow-varying perturbations/uncertainties in the stability derivatives. Here it is assumed that $1 + \bar{d}_i > 0$ and $i = \alpha,\ \delta,\ \Delta$. Random disturbance samples $\bar{d}_{\alpha}$, $\bar{d}_{\delta}$, and $\bar{d}_{\Delta}$ are uniformly distributed in intervals $\pm D_{\alpha}$, $\pm D_{\delta}$, and $\pm D_{\Delta}$, respectively.

Actuator dynamics of divert and attitude thrusters and TVC deflection are given by

$$\dot{\Delta} = \frac{1}{\tau_{\Delta}}(-\Delta + u_{\Delta}), \quad \dot{\delta} = \frac{1}{\tau_{\delta}}(-\delta + u_{\delta}), \quad \dot{\varsigma} = \frac{1}{\tau_{\varsigma}}(-\varsigma + u_{\varsigma}) \tag{5}$$

where δ and Δ are normalized attitude and divert thrusters' forces; ς is TVC deflection; and u_{Δ}, u_{δ}, and u_{ς} are the control inputs to the actuators.

Missile acceleration normal to the velocity vector is related to the flight-path angle rate, without accounting for gravity, as follows:

$$\Gamma = \dot{\gamma} \cdot V \tag{6}$$

The problem is in designing the feedback control law in terms of $\mathbf{u} = \{u_{\Delta}, u_{\delta}, u_{\varsigma}\}^T$ that intercepts a maneuvering target by an impact via driving $r \to 0$ as time increases or providing for $|r(t^*)| \le r^0$ (the r^0 value is to be defined based on the size of the target) that implies the zero intercept at $t_{\text{int}} \le t^*$ in the presence of bounded model uncertainties/disturbances $\bar{d}_{\alpha}$, $\bar{d}_{\delta}$, and $\bar{d}_{\Delta}$ and bounded unknown target accelerations $\Gamma_{\parallel}$ and $\Gamma_{\perp}$. The zero-intercept option can be interpreted as achieving uniform ultimate boundedness (UUB).

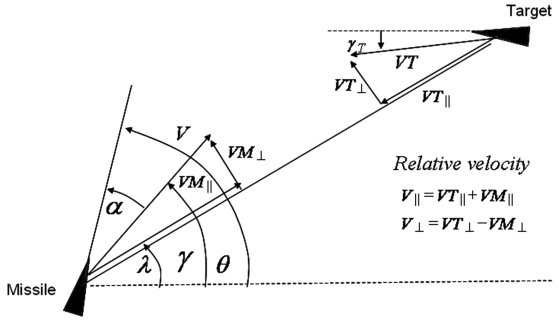

Fig. 3 Interception geometry.

III. Interception Strategy

The following intercept strategy [9,15] that yields a direct hit (zero intercept) is proposed:

$$V_{\perp} = c_0\sqrt{r} \tag{7}$$

where $c_0 > 0$ is some constant.

The viability of the intercept strategy [Eq. (7)] is studied in the following theorem:

Theorem 1: Assume that

1) The intercept strategy in Eq. (7) is enforced by means of the control law $\mathbf{u} = \{u_\Delta, u_\delta, u_\varsigma\}^T$

2) $|\Gamma_\parallel| \le \Gamma_\parallel^{\max}$ and $|\Gamma| \le \Gamma_{\max}$,

then there exist the parameter values $V_\parallel(0) < 0$ and $c_0 > 0$ that make the condition $|r(t^*)| \le r^0$ valid at a given time $t_{\text{int}} \le t^*$.

Proof: Assumption 1 yields the following compensated engagement kinematics [Eq. (1)]:

$$\begin{cases} \dot{r} = V_\parallel \\ \dot{V}_\parallel = c_0^2 + \Gamma_\parallel + \sin(\gamma - \lambda)\Gamma \\ \dot{\lambda} = V_\perp / r \end{cases} \tag{8}$$

Integrating Eq. (8) taking into account assumption 2 and $|\sin(\gamma - \lambda)| < c_1 < 1$, the following inequality is obtained:

$$r(t) \le r(0) + V_\parallel(0)t + \frac{c_0^2 + \Gamma_\parallel^{\max} + c_1\Gamma_{\max}}{2}t^2 \tag{9}$$

The minimal value of $r(t)$ is identified as

$$r(t^*) \le r(0) - \frac{V_\parallel^2(0)}{2(c_0^2 + \Gamma_\parallel^{\max} + c_1\Gamma_{\max})} \tag{10}$$

and zero intercept is achieved at

$$t^* = -\frac{V_\parallel(0)}{(c_0^2 + \Gamma_\parallel^{\max} + c_1\Gamma_{\max})} \tag{11}$$

The parameters $V_\parallel(0) < 0$ and $c_0 > 0$ that yield zero intercept [i.e., $|r(t^*)| \le r^0$] can be selected to meet the condition

$$|V_\parallel(0)| \ge \{2(c_0^2 + \Gamma_\parallel^{\max} + c_1\Gamma_{\max})[r(t^*) - r^0]\} \tag{12}$$

The theorem is proven.

The problem of intercepting a maneuvering target via enforcing the intercept strategy in Eq. (8) is reformulated in terms of sliding mode control. The goal is to design the control law

$$\mathbf{u} = \{u_\Delta, u_\delta, u_\varsigma\}^T \tag{13}$$

that drives the sliding variable

$$\sigma = V_\perp - c_0\sqrt{r} \tag{14}$$

to zero on the trajectory of system 1–5 in finite time.

The multiple-loop integrated guidance–autopilot design is accomplished using SOSM control laws for control and observation. The basics of SOSM techniques that are used for the integrated guidance–autopilot design are studied in the Appendix.

IV. Multiple-Loop Integrated Guidance and Autopilot

A. Control Architecture

The integrated architecture shown in Figs. 4 and 5 consists of seeker, guidance subsystem (outer control loop), and autopilot subsystems (inner control loop). We present thereafter, without loss of generality only the subsystems governing the motions in the pitch plane.

The seeker subsystem performs bore-sight pointing in the line-of-sight (LOS) direction and estimates the rate of change of the LOS and the target acceleration normal to LOS.

The guidance (outer loop) subsystem consists of guidance and inversion that calculate commands for a flight-path angle, an angle of attack, a pitch rate, and an axial thrust. Unlike traditional guidance techniques such as augmented proportional navigation [3] only achieving collision conditions at the end of the interception, the proposed HOSM technique enforces collision conditions mostly through out the entire interception, which reduces the peak interceptor-to-target acceleration advantage.

The autopilot (inner-loop) subsystem includes flight-path angle, pitch-rate, and angle-of-attack autopilots. The angle-of-attack

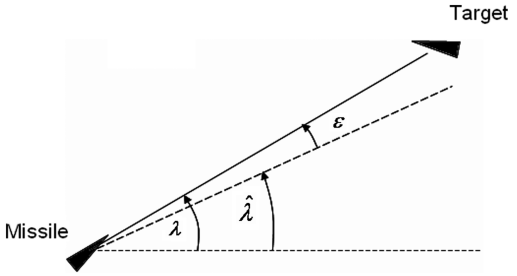

Fig. 4 Seeker bore-sight geometry.

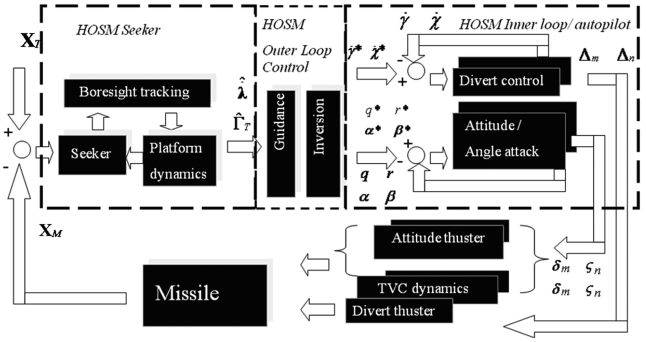

Fig. 5 Guidance and control architecture.

autopilot is used alone during the interceptor fly out; the angle of attack is continuously steered via TVC. During the endgame, the flight-path angle autopilot and the pitch–attitude autopilot are used concurrently. Hit-to-kill accuracy and short time response is achieved by the controlling of the flight-path angle via the firing of divert thrusters. The concurrent tracking by the pitch-rate autopilot of commanded pitch maneuver steers the angle of attack; the corresponding divert lift creates a cooperative disturbance to the flight-path angle autopilot [2], providing a substantial increase of lateral acceleration.

B. Outer (Guidance) Loop Smooth Second-Order Sliding Mode Controller Design

In this section, the chosen sliding variable in Eq. (14) is driven to zero in finite time via SSOSM control designed in terms of Γ in Eqs. (A3) and (A10) format.

The σ-dynamics are identified as

$$\dot{\sigma} = g[V_\parallel(t), V_\perp(t), r(t), \Gamma_\perp(t)] - \cos(\gamma - \lambda)\Gamma \tag{15}$$

where

$$\begin{aligned} g[V_\parallel(t), V_\perp(t), r(t), \Gamma_\perp(t)] &= -V_\parallel V_\perp / r + \Gamma_\perp - c_0 V_\parallel / (2\sqrt{r}) \\ \dot{g}[V_\parallel(t), V_\perp(t), r(t), \Gamma_\perp(t)] &= -\frac{(\dot{V}_\parallel V_\perp + V_\parallel \dot{V}_\perp)r - V_\parallel^2 V_\perp}{r^2} \\ &\quad + \dot{\Gamma}_\perp - \frac{c_0(\dot{V}_\parallel r - V_\parallel^2)}{2r\sqrt{r}} \end{aligned} \tag{16}$$

Also, it is assumed that the variables $V_\parallel(t)$, $V_\perp(t)$, and $r(t)$ are measured, and the function $g[V_\parallel(t), V_\perp(t), r(t), \Gamma_\perp(t)]$ is differentiable with a known Lipschitz constant $L > 0$, which is estimated in Sec. IV.C. The target acceleration transversal to LOS $\Gamma_\perp(t)$ can be estimated by the HOSM observer in Eq. (A3):

$$\begin{aligned} &\dot{z}_0 = v_0 - \cos(\gamma - \lambda)\Gamma - V_\parallel V_\perp - c_0 V_\parallel / (2\sqrt{r}), \\ &v_0 = -2 \cdot L^{1/3}|z_0 - \sigma|^{2/3}\text{sign}(z_0 - \sigma) + z_1, \qquad \dot{z}_1 = v_1, \\ &v_1 = -1.5 \cdot L^{1/2}|z_1 - v_0|^{1/2}\text{sign}(z_1 - v_0) + z_2, \\ &\dot{z}_2 = -1.1 \cdot L \cdot \text{sign}(z_2 - v_1), \qquad \hat{\Gamma}_\perp = z_1 \end{aligned} \tag{17}$$

In the absence of measurement noises, the observer in Eq. (17) provides for exact estimation $\hat{\Gamma}_\perp = \Gamma_\perp$ in finite time [14,15]. If σ and $\cos(\gamma-\lambda)\Gamma + V_\parallel V_\perp + c_0 V_\parallel/(2\sqrt{r})$ are measured with some Lebesgue-measurable noises bounded by $\varepsilon > 0$ and $\varepsilon^{2/3}$ respectively, then [14,15]

$$|z_1(t) - \Gamma_\perp| \le \mu\varepsilon^{2/3}, \qquad \mu > 0 \tag{18}$$

The guidance law that drives $\sigma \to 0$ in finite time is designed in terms of a control input $\Gamma^*(t)$ using SSOSM control [Eqs. (15–17) and (A6)] with $p = 3$ and $m = 2$:

$$\Gamma^* = \frac{1}{\cos(\lambda-\gamma)}\left[\alpha_1|\sigma|^{1/2}\text{sign}(\sigma) + \alpha_2\int|\sigma|^{1/3}\text{sign}(\sigma)\,d\tau - N'\frac{V_\perp V_\parallel}{r} - \frac{c_0 V_\parallel}{2\sqrt{r}} + \hat{\Gamma}_\perp\right], \qquad N' = 1 \tag{19}$$

Remark 1: The term $-N'\frac{V_\parallel V_\perp}{r} = -N' V_\parallel \omega_\lambda$ is known as proportional navigation guidance [3].

Rewriting Eq. (19) as

$$\begin{cases} \Gamma^* = \frac{1}{\cos(\lambda-\gamma_M)}(-N'\frac{V_r V_\lambda}{r} + U_d + \hat{\Gamma}_\perp), \qquad N' = 4 \\ U_d = \alpha_1|\sigma|^{1/2}\text{sign}\,\sigma + \alpha_2\int|\sigma|^{1/3}\text{sign}(\sigma)\,d\tau - \frac{c_0 V_\parallel}{2\sqrt{r}} \end{cases} \tag{20}$$

one can interpret the SSOSM guidance law as pseudoproportional navigation guidance with the term U_d providing the finite-time convergence in the absence of the measurement noise. The guidance coefficient $N' = 1$ in Eq. (19) is taken as $N' = 4$ in Eq. (20) to have an adequate comparison of the SSOSM guidance law given by Eq. (20) and the traditional proportional navigation guidance law.

C. Evaluation of the Lipschitz Constant for the Outer (Guidance) Loop

It is assumed that the target acceleration transversal to the line of sight $\Gamma_\perp(t)$ is differentiable. Then the function $g[V_\parallel(t), V_\perp(t), r(t), \Gamma_\perp(t)]$ is also differentiable, and the function $\dot{g}[V_\parallel(t), V_\perp(t), r(t), \Gamma_\perp(t)]$ is continuous everywhere except for $r = 0$. This singularity point occurs when intercept by impact happens. However, technically, the intercept by impact (hit to kill) happens when $r \ne 0$ but belongs to the interval [6,7] $r \in [r_{\min}, r_{\max}] = [0.1, 0.25]$ m. This fact is due to a certain size of the ballistic target, and a particular intercept value of $r^0 \in [0.1, 0.25]$ m, named zero intercept, depends on this size. Therefore, the function $g[V_\parallel(t), V_\perp(t), r(t), \Gamma_\perp(t)]$ is differentiable and the function $\dot{g}[V_\parallel(t), V_\perp(t), r(t), \Gamma_\perp(t)]$ is continuous everywhere until hit-to-kill zero intercept happens. Its Lipschitz constant is estimated in the following theorem:

Theorem 2: Assume that

$$|\Gamma| \le \Gamma_{\max}, \quad |\dot{\Gamma}_\perp| \le \dot{\Gamma}_\perp^{\max}, \quad |\Gamma_\perp| \le \Gamma_\perp^{\max}, \quad |\Gamma_\parallel| \le \Gamma_\parallel^{\max}$$
$$|V_\perp(t)| \le V_\perp^{\max}, \quad V_\parallel(0) = M \ll 0, \quad M \le V_\parallel(t) \le 0$$

in a reasonable flight domain, then the Lipschitz constant L for $\dot{g}[V_\parallel(t), V_\perp(t), r(t), \Gamma_\perp(t)]$ can be estimated as

$$L \approx \dot{\Gamma}_\perp^{\max} + \frac{V_\perp^{\max}}{(r^0)^2}[(V_\perp^{\max})^2 + 2M^2] \tag{21}$$

Proof: Using Eq. (16) and taking into account inequalities $|\sin(\lambda-\gamma_M)| < c_1 < 1$, and $|\cos(\lambda-\gamma_M)| < c_2 < 1$ the following inequality holds:

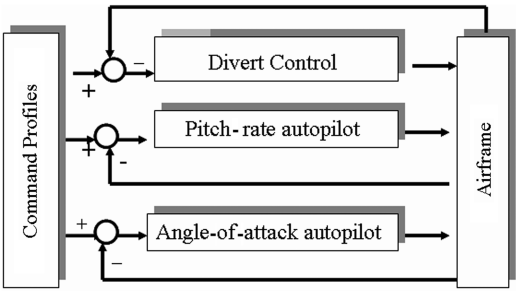

Fig. 6 Interceptor autopilot architecture.

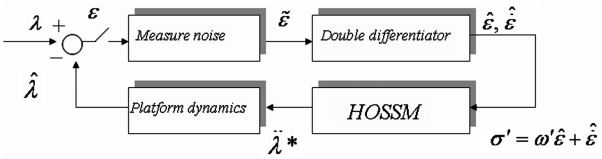

Fig. 7 Seeker bore-sight tracking architecture.

$$\begin{aligned} &|\dot{g}[V_\parallel(t), V_\perp(t), r(t), \Gamma_\perp(t)]| \\ &\le \dot{\Gamma}_\perp^{\max} + \frac{|(\dot{V}_\parallel V_\perp + V_\parallel \dot{V}_\perp)r - V_\parallel^2 V_\perp|}{r^2} + \frac{c_0|(\dot{V}_\parallel r - V_\parallel^2)|}{2r\sqrt{r}} \\ &\le \dot{\Gamma}_\perp^{\max} + \frac{1}{(r^0)^2}\left[(V_\perp^{\max})^3 + 2M^2 V_\perp^{\max} + \frac{c_0\sqrt{r^0}}{2}(V_\perp^{\max} + M^2)\right] \\ &+ \frac{1}{r^0}\left[(\Gamma_\perp^{\max} + c_1\Gamma_{\max})V_\perp^{\max} + |M|(\Gamma_\perp^{\max} + c_2\Gamma_{\max})\right. \\ &\left. + \frac{c_0\sqrt{r^0}}{2}(\Gamma_\perp^{\max} + c_1\Gamma_{\max})\right] = L \end{aligned}$$

Because $0 < r^0 \ll 1$ then

$$L \approx \dot{\Gamma}_\perp^{\max} + \frac{V_\perp^{\max}}{(r^0)^2}[(V_\perp^{\max})^2 + 2M^2]$$

and the theorem is proven.

D. Inversion

Figure 6 represents the relation of the inversion with the flight-path angle, pitch-rate, and angle-of-attack autopilots. First of all, command profiles γ^*, $\dot{\gamma}^*$, and $\ddot{\gamma}^*$ are computed in real time

$$\dot{\gamma}^*(t) = \frac{\Gamma^*(t)}{V}, \qquad \ddot{\gamma}^*(t) = \frac{\dot{\Gamma}^*(t)}{V}, \qquad \gamma^*(t) = \frac{1}{V}\int_0^t \Gamma^*(\tau)\,d\tau, \qquad \gamma(0) = \gamma_0 \tag{22}$$

where $\Gamma^*(t)$ is assumed to be differentiable. Second, the angle-of-attack command profile α^* and its derivative are computed in real

Table 1 Interception geometry

Variable	Description	Value
$\lambda(0)$	Initial LOS angle, rad	0.1
$\gamma(0) - \lambda(0)$	Initial lead angle, rad	0.1
$\gamma(0)$	Initial interceptor flight-path angle, rad	0.3
$\gamma_T(0)$	Initial target flight-path angle, rad	−0.02
$V_T(0)$	Initial target velocity, m/s	5000
V	Initial and terminal interceptor velocities, m/s	2500–4800
$Z(0)$	Initial interceptor altitude, m	30,000
$Z_T(0)$	Initial target altitude,	65,000
$X(0)$	Initial interceptor longitudinal position,	0
$X_T(0)$	Initial target longitudinal position,	350,000
β_T	Target ballistic coefficient, lb/ft^2	500–1500

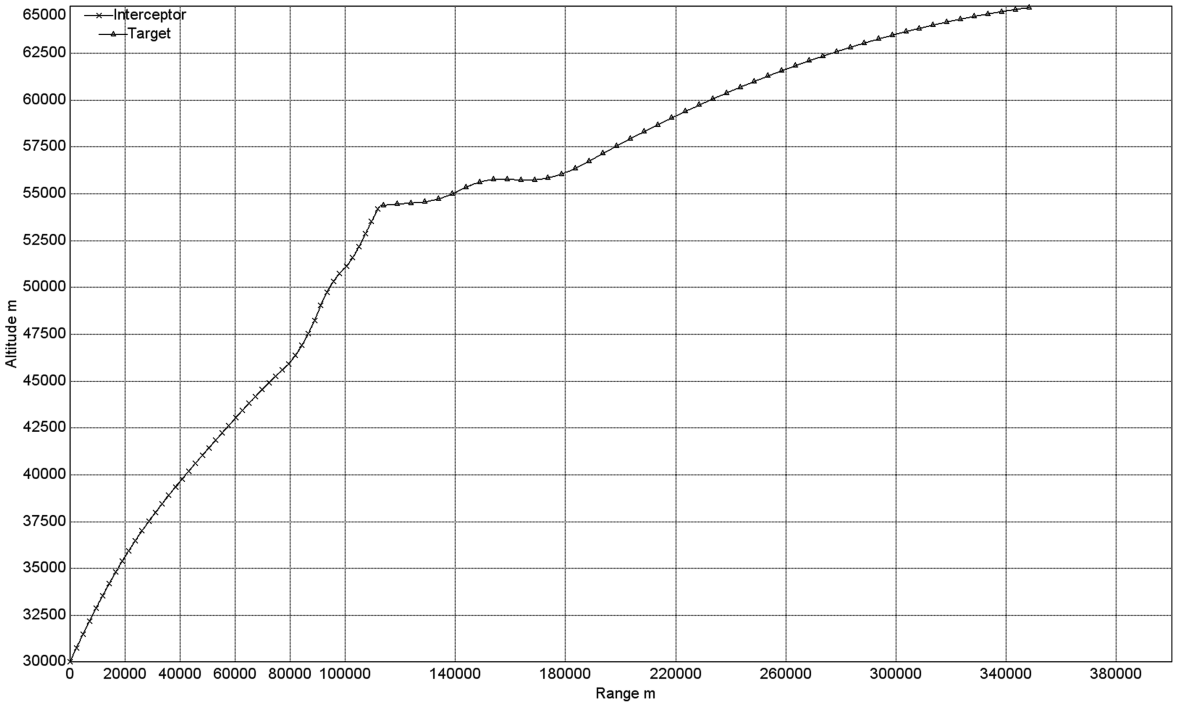

Fig. 8 Interception geometry.

time assuming full knowledge of the stability derivatives Z_α and $\dot{\gamma}^*(t)$, although nullifying the direct effect of attitude and divert thrusts δ and Δ in Eqs. (2–5):

$$\alpha^* = \begin{cases} \frac{1}{Z_\alpha}[\dot{\gamma}^* + \frac{g}{V}\cos(\gamma^*)], & \text{if } |\frac{1}{Z_\alpha}[\dot{\gamma}^* + \frac{g}{V}\cos(\gamma^*)]| \le \alpha_{\max} \\ \alpha_{\max}, & \text{if } |\frac{1}{Z_\alpha}[\dot{\gamma}^* + \frac{g}{V}\cos(\gamma^*)]| > \alpha_{\max} \\ -\alpha_{\max}, & \text{if } |\frac{1}{Z_\alpha}[\dot{\gamma}^* + \frac{g}{V}\cos(\gamma^*)]| < -\alpha_{\max} \end{cases} \quad (23)$$

$$\dot{\alpha}^* = \begin{cases} \frac{1}{Z_\alpha}[\ddot{\gamma}^* - \frac{g}{V}\dot{\gamma}^*\sin(\gamma^*) - \frac{g\dot{V}}{2}\cos(\gamma^*)], & \text{if } |\alpha^*| < \alpha_{\max} \\ 0, & \text{otherwise} \end{cases} \quad (24)$$

The corresponding pitch-rate command q^* is calculated in real time:

$$q^* = \dot{\alpha}^* + \dot{\gamma}^* \quad (25)$$

The pitch-rate command profile q^* is supposed to be followed by aerodynamic thruster control u_δ. Clearly, $q \to q^*$ implies approximate following $\alpha \to \alpha^*$ while creating a cooperative disturbance term $Z_\alpha\alpha$ in Eq. (4), and, thus, owing to the robustness of SOSM accuracy following $\alpha \to \alpha^*$ is not required.

Remark 2: It is worth noting that tracking α^* does not imply an accurate tracking of $\dot{\gamma}^*$, because the purpose of the attitude thruster's control is only to generate an aerodynamic maneuver, which in effect is a cooperative disturbance that alleviates the divert thruster's control. Next, the difference between γ^* and γ is steered to zero by the divert thrusters control u_Δ in the presence of this cooperative disturbance thereby increasing significantly (up to 100%) the missile's overall divert maneuver capability.

E. Second-Order Nonlinear Dynamic Sliding Manifold-Based Flight-Path Angle Autopilot

Equations (2–5) have the vector relative degree [2,2,2] with respect to the vector output $y = \{\gamma, q, \alpha\}^T$. This calls for SOSM algorithms that are able to drive corresponding sliding variables and their derivatives to zero in finite time.

Remark 3: It is assumed that the missile mathematical model in Eqs. (2–5) is of a minimum or slightly nonminimum phase. Otherwise, one may apply the techniques described in [9].

The flight-path angle sliding variable is introduced:

$$\sigma_\gamma = \varepsilon_\gamma + \varpi\int_0^t \varepsilon_\gamma(\tau)\,\mathrm{d}\tau, \qquad \varepsilon_\gamma = \gamma^* - \gamma, \qquad \varpi = 50\ \mathrm{rad/s} \quad (26)$$

Table 2 Missile characteristics

Variable	Description	Value
$m0$, m	Interceptor initial, final mass, kg	1400–100
J_{yy}	Pitch moment of inertia, kg · m^2	372–4
V	Interceptor initial final longitudinal velocity, m/s	2500–4800
C_{L_α}	Lift gradient coefficient	4
a_α	Distance of the aerodynamic center from the c.g. along the x-body axis, m	0.05
a_δ, a_ζ	Distance of the application point of attitude thrust and of the sustainer from the c.g. along the x-body axis, m	0.4, −0.8
a_Δ	Distance of the application point of divert thrust from the c.g. along the x-body axis, m	0.02
$T_{\max\delta}$	Nominal magnitude of attitude thrust, N	3000
$T_{\max\Delta}$	Nominal magnitude of divert thrust, N	30,000
T_s	Sustainer thrust, N	100,000
D_α, D_δ, D_Δ	Maximum magnitude of aerodynamic lift, attitude, and divert thrust relative disturbances	0.3
S	Reference surface, m^2	0.4 − 0.0707
$\bar{C}$	Reference length, m	0.7 − 0.3
$\alpha_{\max}$	Maximum value of commanded angle-of-attack profile, rad	0.5
τ_δ, τ_Δ, τ_ζ	Attitude and divert thrusters time constant, s	0.005, 0.005, 0.05

Equation (26) shows that, once the sliding surface $\sigma_\gamma = 0$ is achieved in finite time, $\varepsilon_\gamma \to 0$ asymptotically. The following σ_γ input–output dynamics are derived:

$$\ddot{\sigma}_\gamma = f_\gamma(t) - b_\Delta u_\Delta \tag{27}$$

where

$$\begin{cases} f_\gamma(t) = \ddot{\gamma}^* + \varpi\dot{\gamma}^* + [Z_\alpha(1+\bar{d}_\alpha) - Z_\delta(1+\bar{d}_\delta)\sin(\alpha)\delta - Z_q q \\ Z_\Delta(1+\bar{d}_\Delta)\sin(\alpha)\Delta]\dot{\alpha} + (\frac{g}{V}\sin(\gamma) - \varpi)\dot{\gamma} \\ +Z_\delta(1+\bar{d}_\delta)\cos(\alpha)\dot{\delta} - \frac{Z_\Delta(1+\bar{d}_\Delta)\cos(\alpha)}{\tau_\Delta}\Delta, \qquad b_\Delta = \frac{Z_\Delta(1+\bar{d}_\Delta)\cos(\alpha)}{\tau_\Delta} \end{cases}$$

It is assumed that the disturbance $f_\gamma(t)$ is bounded in an operational domain Ω_γ: $|f_\gamma(t)| \le L_\gamma$, as well as $|\bar{d}_\Delta| < 1$, $Z_\Delta > 0$ and $|\alpha| \le 0.5$, then $b_\Delta > 0$, $b'_\Delta < b_\Delta < b''_\Delta$, and the divert thrust controller based on the SOSM/NDSM (nonlinear dynamic sliding manifold) is designed in a form [Eq. (A10)] as

$$\begin{cases} \dot{\chi}_\gamma = \xi_\gamma|\sigma_\gamma|^{0.5}\text{sign}\,(\sigma_\gamma) - \eta_\gamma|J_\gamma|^{0.5}\text{sign}\,(J_\gamma) \\ J_\gamma = \chi_\gamma + \sigma_\gamma, \qquad u_\Delta = \bar{\rho}_\gamma \cdot \text{sign}\,(J_\gamma) \end{cases} \tag{28}$$

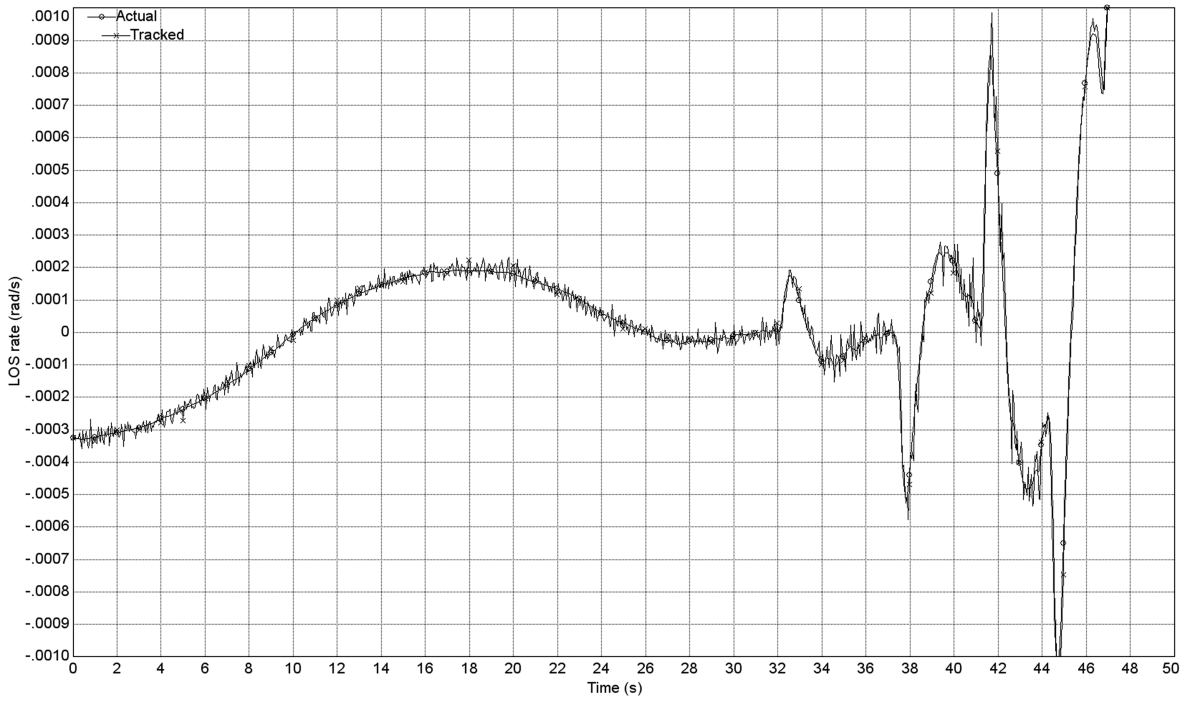

a)

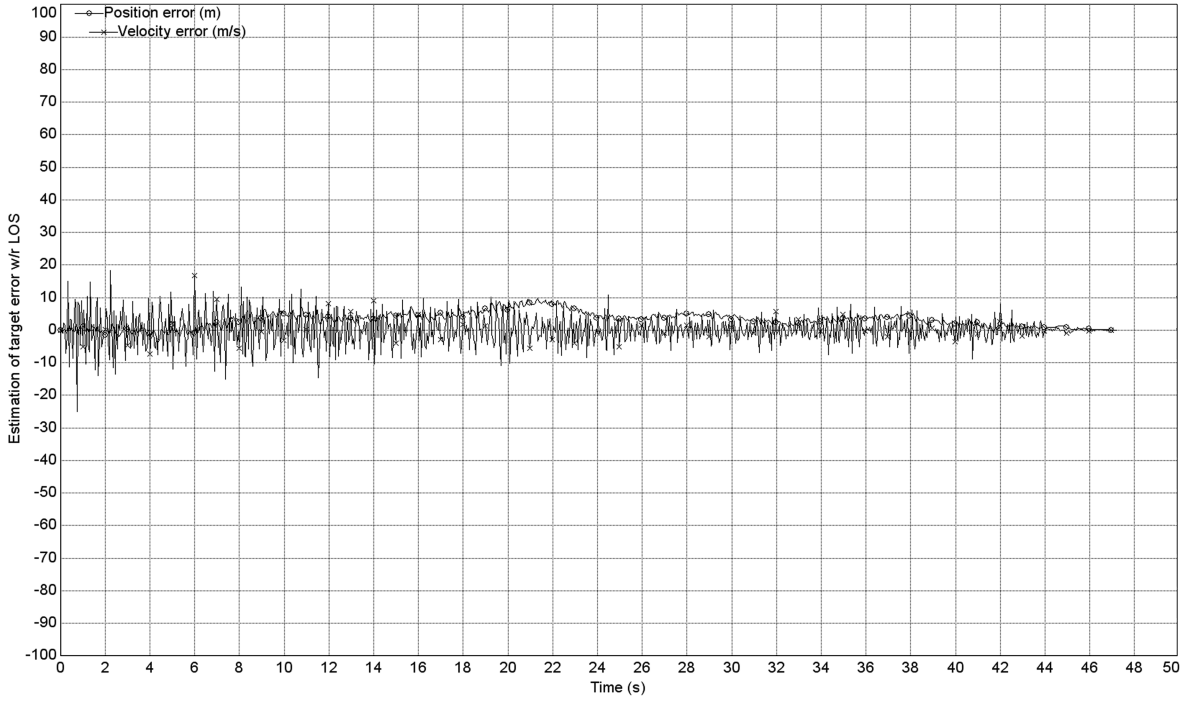

b)

Fig. 9 Illustrations of a) actual and estimated bore-sight angle rate and b) accuracy of LOS and LOS rate estimation.

F. Second-Order Nonlinear Dynamic Sliding Manifold-Based Pitch-Rate Autopilot

Following the SOSM/NDSM control design technique the pitch-rate sliding variable is introduced:

$$\sigma_q = \varepsilon_q + \varpi' \int_0^t \varepsilon_q(\tau)\,\mathrm{d}\tau, \qquad \varepsilon_q = q^* - q, \qquad \varpi' = 20\ \mathrm{rad/s} \quad (29)$$

Equation (29) shows that, once the sliding surface $\sigma_q = 0$ is achieved at the finite time, the pitch-rate tracking error ε_q converges to zero asymptotically according to the eigenvalue of $\sigma_q = 0$. Differentiating twice Eq. (29) gives

$$\ddot{\sigma}_q = f_q(t) - b_\delta u_\delta \quad (30)$$

where

$$\begin{cases} f_q(t) = \ddot{q}^* + \varpi' \dot{q}^* - M_\alpha(1+\bar{d}_\alpha)\dot{\alpha} - (M_q + \varpi)\dot{q} \\ -M_\Delta(1+\bar{d}_\Delta)\dot{\Delta} + \frac{M_\delta d_\delta}{\tau_\delta}(1+\bar{d}_\delta)\delta; \\ b_\delta = \frac{M_\delta(1+\bar{d}_\delta)}{\tau_\delta} \end{cases}$$

It is worth noting that the thrust vectoring terms containing ς are removed, because thrust vectoring is not used altogether with attitude thrusters. One can easily show that the disturbance $f_q(t)$ is bounded in an operational domain Ω_q: $|f_q(t)| \le L_q$. Because it is assumed that $|\bar{d}_\delta| < 1$ and $M_\delta > 0$ then $b_\delta > 0$ and $b'_\delta < b_\delta < b''_\delta$, and the SOSM/NDSM control in Eq. (A10) can be employed for stabilizing σ_q and its derivative $\dot{\sigma}_q$ at zero in finite time. Corresponding SOSM/NDSM-based attitude thrust controller is given by

$$\begin{cases} \dot{\chi}_q = \xi_q |\sigma_q|^{0.5} \mathrm{sign}\,(\sigma_q) - \eta_q |J_q|^{0.5} \mathrm{sign}\,(J_q) \\ J_q = \chi_q + \sigma_q, \qquad u_\delta = \bar{\rho}_q \cdot \mathrm{sign}\,(J_q) \end{cases} \quad (31)$$

G. Second-Order Nonlinear Dynamic Sliding Manifold-Based Angle-of-Attack Autopilot

It is worth noting that $\max|Z_\delta\delta + Z_\Delta\Delta| \ll \max|q|$ and $\max|M_\delta| \gg \max|M_\Delta|$. This means that the missile angle of attack α is mostly governed by the pitch rate q, which itself is controlled by the attitude thrusters force δ. The sliding surface σ_α is defined

$$\sigma_\alpha = \varepsilon_\alpha + \varpi'' \int_0^t \varepsilon_\alpha\,\mathrm{d}\tau, \qquad \varepsilon_\alpha = \alpha^* - \alpha, \qquad \varpi'' = 20\ \mathrm{rad/s} \quad (32)$$

Differentiating Eq. (32) twice with respect to time yields

$$\ddot{\sigma}_\alpha = f_\alpha(t) - b_\varsigma u_\varsigma \quad (33)$$

where one can show that similar to Eq. (30) $f_\alpha(t)$ is a bounded variable, whereas $b_\varsigma = M_\varsigma/\tau_\varsigma$. The angle-of-attack TVC is supposed to be continuous in addition to being robust to the disturbances. The supertwisting continuous control is designed in accordance with Eqs. (A12) and (A14):

$$\begin{cases} u_\varsigma = \frac{1}{b_\varsigma}[-\xi_\alpha |S_\alpha|^{1/2} \mathrm{sign}\,(S_\alpha) + w_\varsigma] \\ \dot{w}_\varsigma = -\eta_\alpha\,\mathrm{sign}\,(S_\alpha) \end{cases} \quad (34)$$

where the auxiliary sliding variable is introduced as

$$S_\alpha = \dot{\sigma}_\alpha + c_\alpha \sigma_\alpha, \qquad c_\alpha > 0 \quad (35)$$

H. Seeker Tracking Using SOSM Techniques

We assume that the seeker is gimbaled as represented Fig. 7. Because of seeker measurement errors, seeker measurements are extremely noisy, and yet the input to the guidance must be smooth. Given the very long range of the interceptor, the seeker includes several optics allowing for adjusting the pixel size function of the range.

Actual LOS angle in the pitch plane is represented in Fig. 3 by λ; and the seeker bore sight is represented in the pitch plane by $\hat{\lambda}$ and corresponding error $\varepsilon = \lambda - \hat{\lambda}$. The seeker processes a noisy measurement $\tilde{\varepsilon} = \varepsilon + \delta\varepsilon$ and generates angular acceleration command $\ddot{\lambda}^*$ to the platform bearing the seeker; the dynamics thereof are represented by

$$\hat{\lambda} = \frac{1}{s^2} \frac{\ddot{\lambda}^* \omega'''^3}{s^3 + 1.75\omega''' s^2 + 2.15\omega'''^2 s + \omega'''^3} \quad (36)$$

where s is a Laplace variable. The seeker samples measurement and introduces measurement errors; corresponding output is $\tilde{\varepsilon}$ as shown in Fig. 7. Given the extreme unsmoothness of the error signal, it is prefiltered by a sixth-order bandpass filter hereafter:

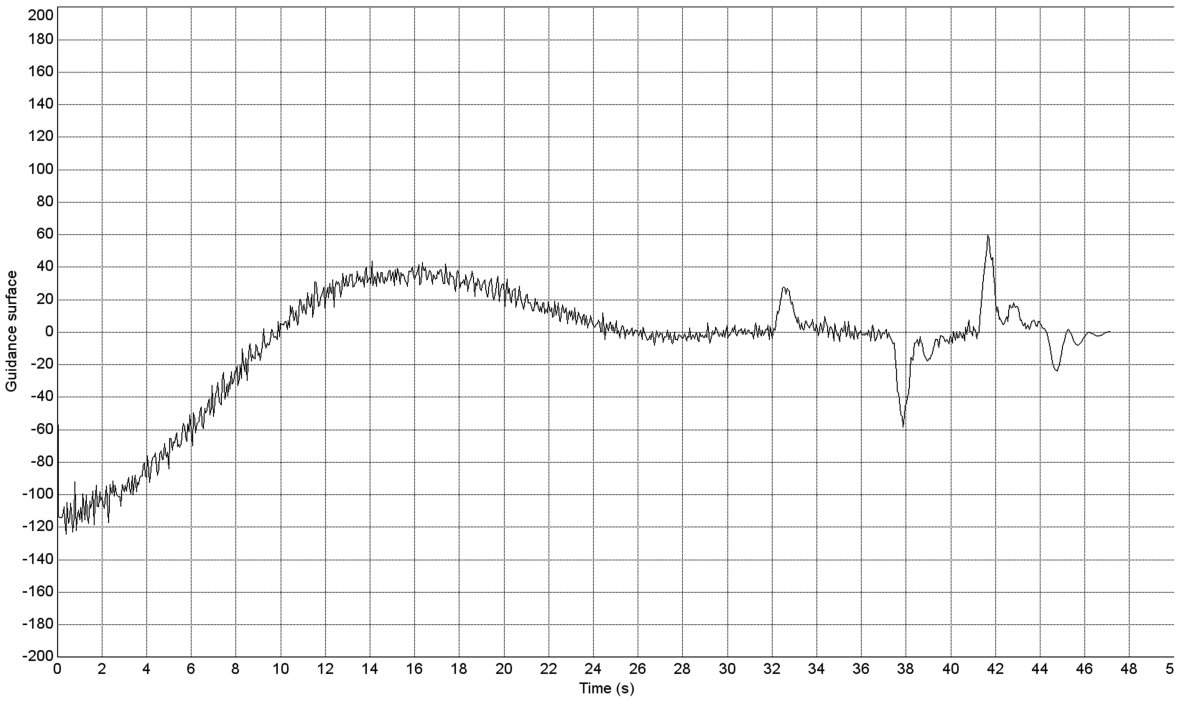

Fig. 10 Guidance sliding surface with step maneuvers.

$$\tilde{\varepsilon}=\frac{\tilde{\varepsilon}\omega^6}{s^6+3.25\omega s^5+6.6\omega^2 s^4+8.6\omega^3 s^3+7.45\omega^4 s^2+3.95\omega^5 s+\omega^6}$$
$$\omega=50\,\text{rad/s} \tag{37}$$

The SOSM/NDSM differentiator [20,21] that estimates and filters $\hat{\varepsilon}$ and $\dot{\hat{\varepsilon}}$ is given by

$$\begin{cases}\dot{\hat{\tilde{\varepsilon}}}=\rho_0\,\text{sign}\,(J_0)\\ \dot{\chi}=b|\tilde{\varepsilon}-\hat{\varepsilon}|^{1/2}\text{sign}\,(\tilde{\varepsilon}-\hat{\varepsilon})-a|J_0|^{1/2}\text{sign}\,(J_0)\\ J_0=\chi+\tilde{\varepsilon}-\hat{\varepsilon}\end{cases} \tag{38}$$

where J_0 is the NDSM, and the coefficients $a>b>0$ and $\rho_o>0$ are sufficiently large.

Both outputs $\hat{\varepsilon}$ and $\dot{\hat{\varepsilon}}$ are bandpass-filtered for the sake of smoothness using a third-order filter:

$$\underline{y}=\frac{y\omega''^3}{s^3+1.75\omega'' s^2+2.15\omega''^2 s+\omega''^2},\quad y=\hat{\varepsilon},\dot{\hat{\varepsilon}},\quad \omega''=50\,\text{rad/s} \tag{39}$$

The bore-sight sliding variable σ' is introduced:

$$\sigma'=\dot{\hat{\varepsilon}}+\varpi'''\hat{\varepsilon}=0 \tag{40}$$

And its dynamics are derived:

$$\dot{\sigma}'=g(.)-\dddot{\lambda}^* \tag{41}$$

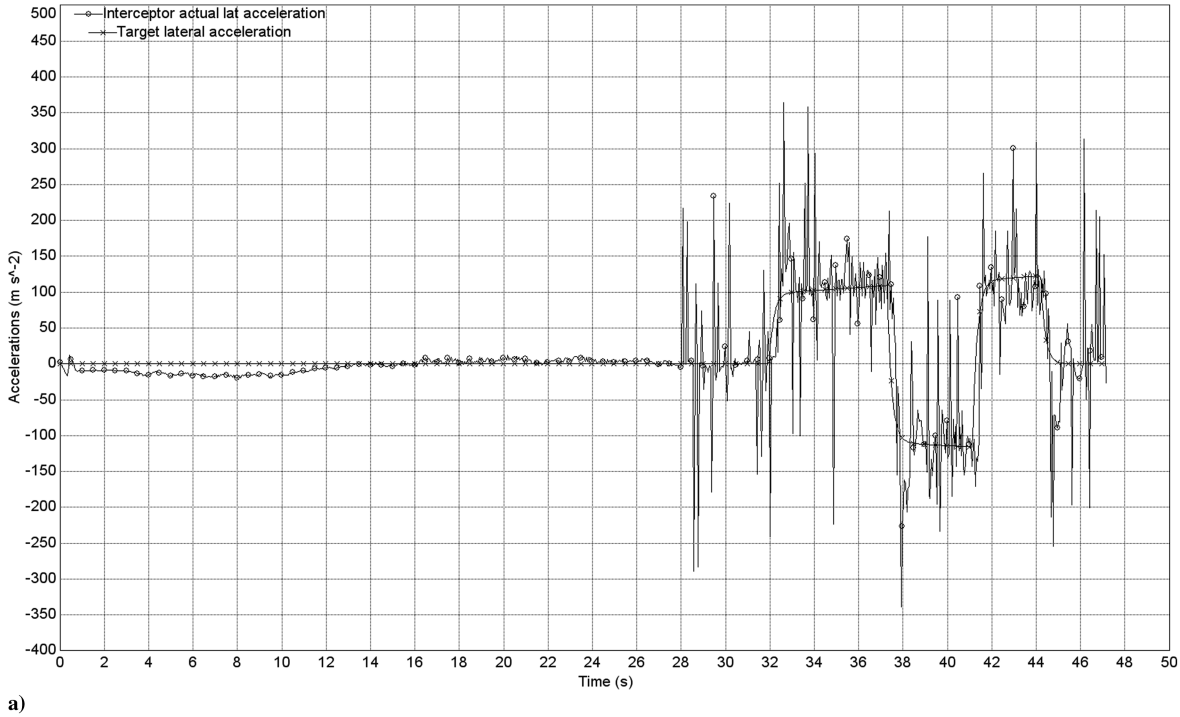

a)

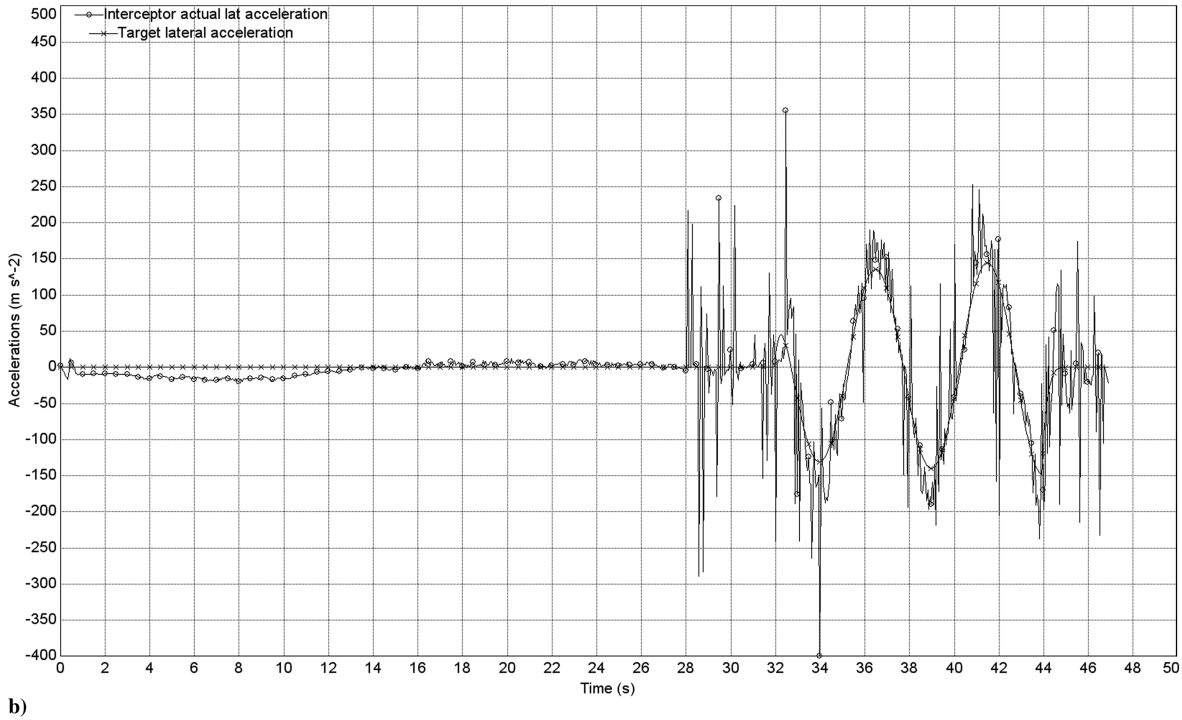

b)

Fig. 11 Illustrations of a) comparison of interceptor and target step maneuvers and b) comparison of interceptor and target wave maneuvers.

with $g(.)$ representing a disturbance. The continuous angular acceleration command $\ddot{\lambda}^*$ to the bore sight, which drives $\sigma' \to 0$ in finite time, $\hat{\varepsilon}$, $\dot{\hat{\varepsilon}} \to 0$, and $\hat{\lambda} \to \lambda$ as time increases, is derived in SSOSM format [Eqs. (A3) and (A7)]:

$$\ddot{\lambda}^* = z_1 + \alpha_1 |\sigma'|^{0.5} \text{sign}(\sigma') + \alpha_2 \int_0^t |\sigma'|^{0.5} \text{sign}(\sigma')\, d\tau$$

$$\dot{z}_0 = v_0 - \dddot{\hat{\lambda}}, \qquad v_0 = -2 \cdot \bar{L}^{1/3} |z_0 - \sigma'|^{2/3} \text{sign}(z_0 - \sigma') + z_1 \quad (42)$$

$$\dot{z}_1 = v_1, \qquad v_1 = -1.5 \cdot \bar{L}^{1/2} |z_1 - v_0|^{1/2} \text{sign}(z_1 - v_0) + z_2$$

$$\dot{z}_2 = 1.1 \cdot \bar{L} \cdot \text{sign}(z_2 - v_1)$$

with $|\ddot{\bar{g}}(.)| \le \bar{L}$. Finally, the target acceleration component normal to bore sight is estimated as

$$\hat{\Gamma}_\perp = z_1 r + \varpi''' \dot{\hat{\varepsilon}} r + 2V_\parallel (\dot{\hat{\lambda}} + \dot{\hat{\varepsilon}}) + \hat{\varepsilon} \dot{V}_\parallel + \Gamma \cos(\hat{\lambda} - \gamma) \quad (43)$$

V. Simulation

A. Simulation Setup

The parameters of the endoatmospheric interception geometry missile are given in the Table 1. The target undergoes either sinusoidal maneuvers with frequencies and amplitudes varying with

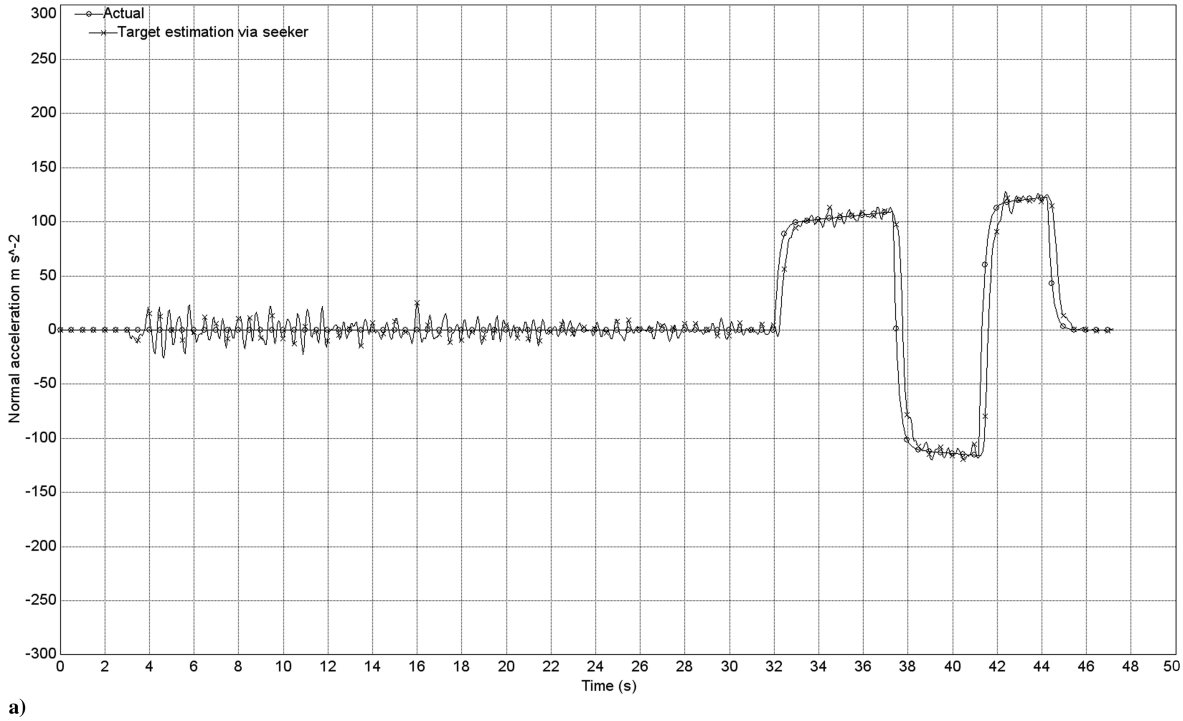

a)

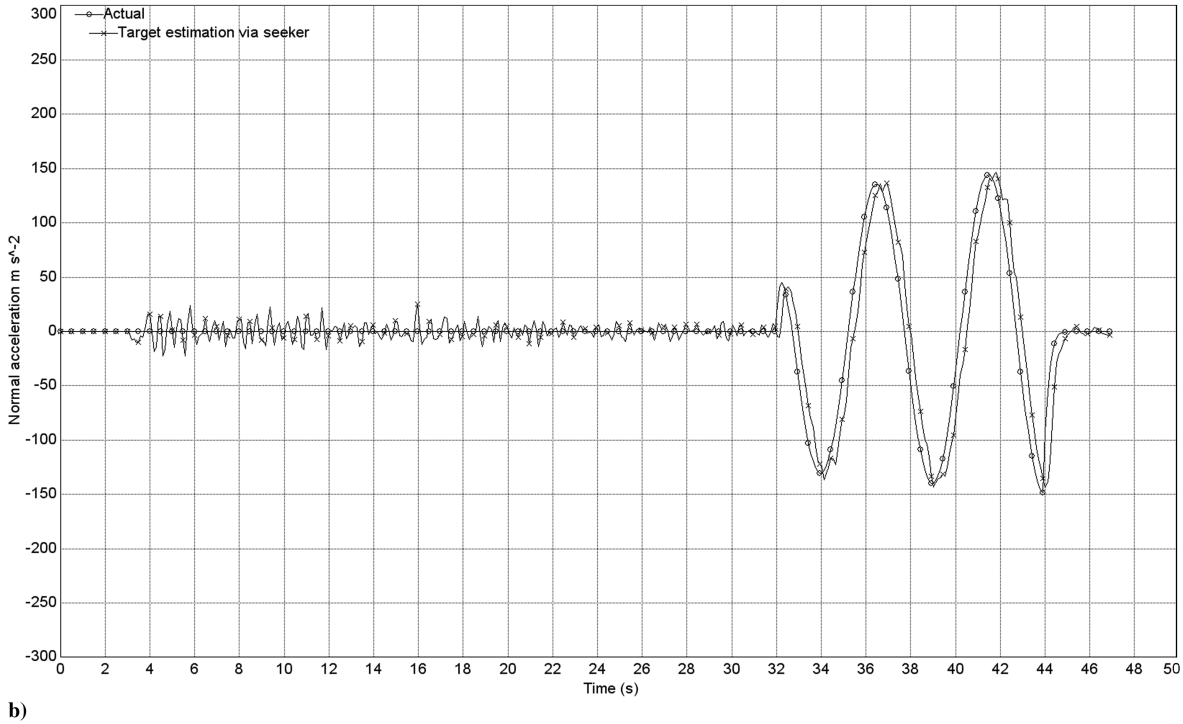

b)

Fig. 12 Illustrations of a) estimation of target normal step acceleration maneuvers and b) estimation of target normal wave acceleration maneuvers.

altitude in the 200–300 m/s^2 range or step maneuvers with changing polarity. Target longitudinal motion is governed by a ballistic coefficient varying with altitude between values of 1500 to 500 lbf/ft^2. Although SI units are consistently used in this work, the ballistic coefficient is given in lbf/ft^2 to ease the reader. For time $t \leq 27.9$ s the interceptor is accelerated by the sustainer thrust with its attitude being steered by thrust vectoring; thereafter, the attitude is steered by attitude thrusters and lateral divert is achieved by the combined effects of aerodynamic lift and on–off divert thrusters. The intercept geometry is shown in Fig. 8.

The parameters of a dual-thrust-controlled endoatmospheric missile are given in the Table 2.

For ranges larger than 25 km single pixel measurements are made. A pixel size is set to 50 μrad when the range is greater than 100 km. For ranges less than 100 km and greater than 50 km the pixel size is 100 μrad, for pixel sizes less than 50 km and greater than 25 km pixel size is 200 μrad. When the range r is less than or equal to 25 km, it is assumed that the target extends over several pixels and the measurements errors are governed by a normal distribution with a standard deviation of 50 μrad.

Table 2 shows that due to the position of the center of pressure ahead of the center of gravity the interceptor is naturally unstable. It is worth noting that the missile autopilot may experience time delays due to onboard computer latency. Special methods that mitigate the

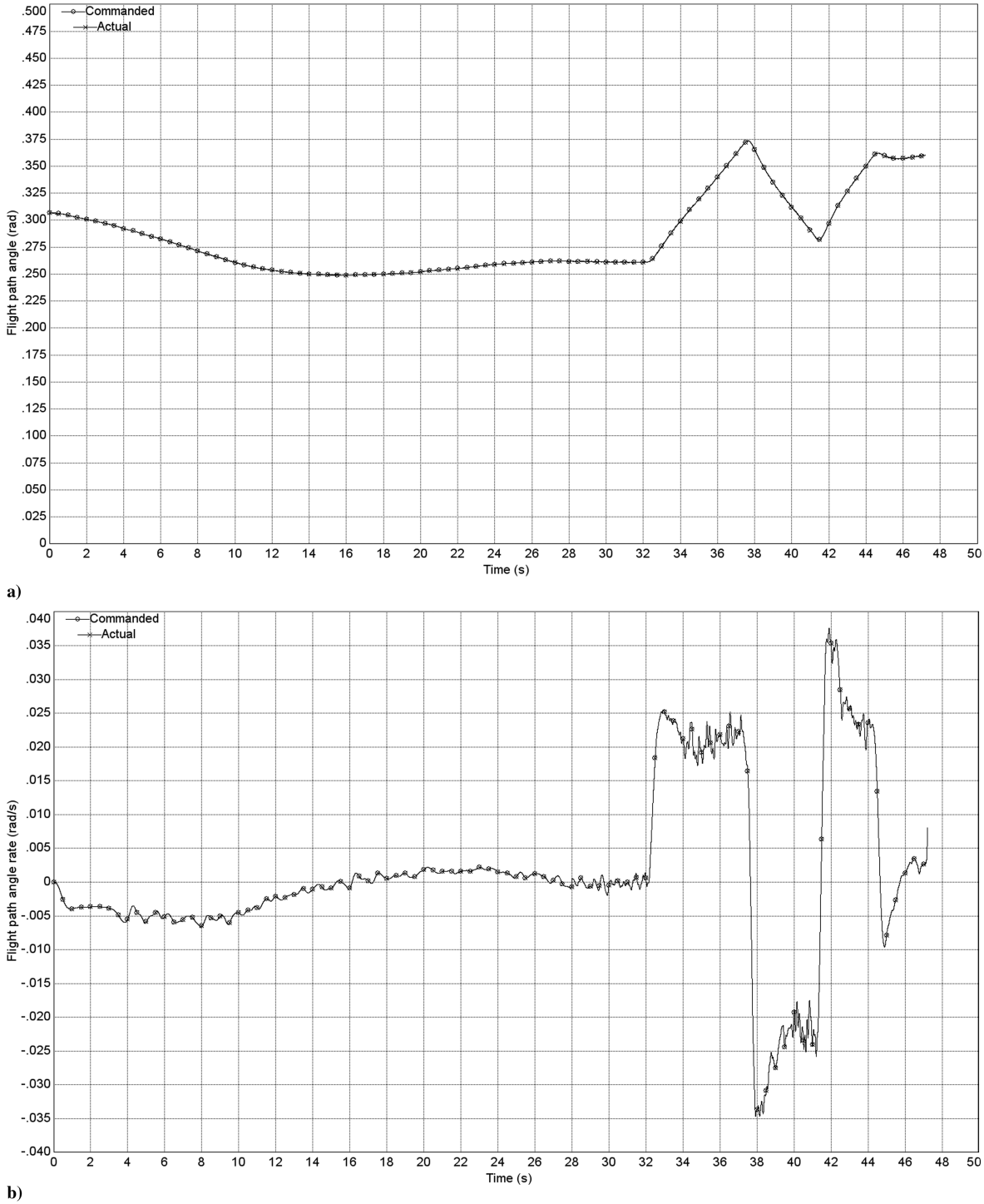

Fig. 13 Illustrations of a) flight-path angle tracking and b) flight-path angle rate tracking.

time-delay problem are developed for sliding mode control [17]. In this work the simulations are performed with 3 ms time delay in guidance command in Eq. (20) and 2 ms time delay in the autopilot commands in Eqs. (28), (31), and (34).

B. Bore-Sight Tracking Performance

Plots in Fig. 9a show that once the guidance sliding surface is reached the LOS rate remains extremely small, less than 2 mrad/s. Results in Fig. 9b show that notwithstanding large seeker errors of up to 200 μrad uniformly distributed errors, the tracking of LOS and LOS rates are excellent: in the 20 μrad with a brief 50 μrad/s peak at the end of the interception.

C. Guidance Results

The plots in Fig. 10 were obtained against a waiving target. They show that the sliding surface is reached after 25 s and that the sliding motion is kept thereafter with short departures during the maneuvers. The mean magnitude of the surface is less than 3–5 m/s. This can be interpreted as a velocity error in the collision condition. If one propagates such error over the settling time of the flight-path rate autopilot, that is 0.08 s, one finds a miss distance of 0.3 m consistent

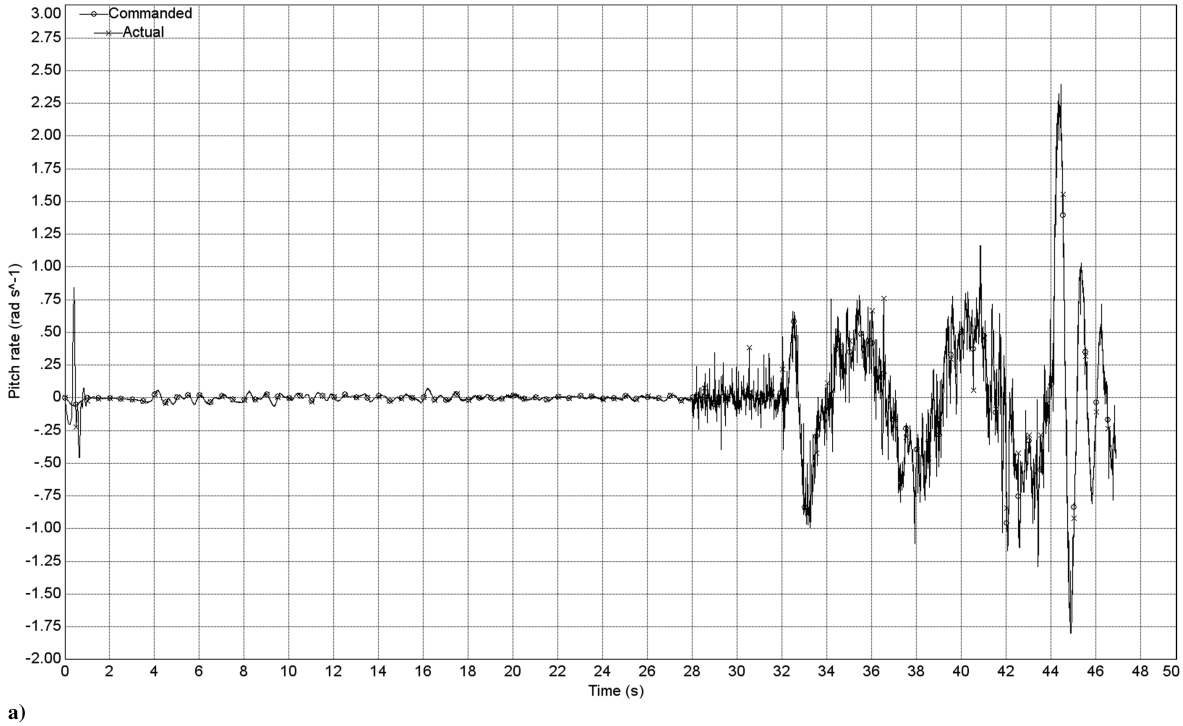

a)

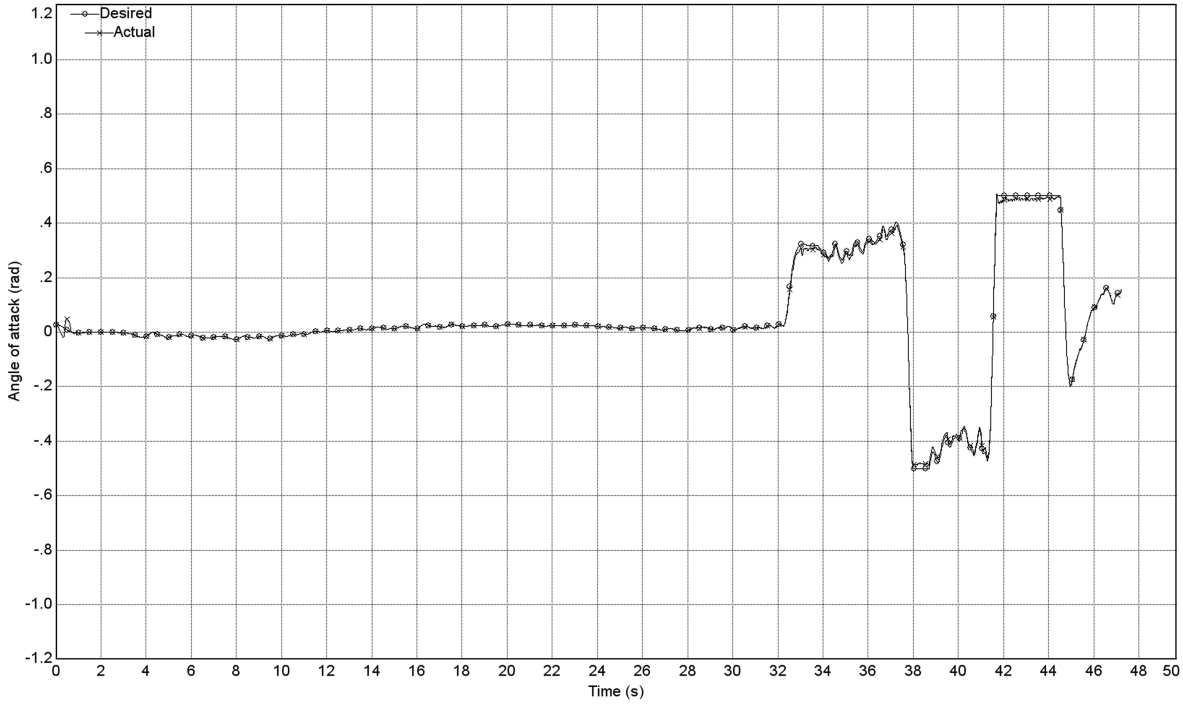

b)

Fig. 14 Illustrations of a) pitch-rate tracking performance and b) angle-of-attack tracking performance.

with the actual miss distance of 0.15 m. Plots in Figs. 11a and 11b show that interceptor acceleration mimics very closely the target acceleration for wave and step maneuvers.

D. Estimation of Target Normal Acceleration

Target normal acceleration is estimated using the HOSM observer for the seeker bore-sight pointing in Eq. (43). It is also estimated by

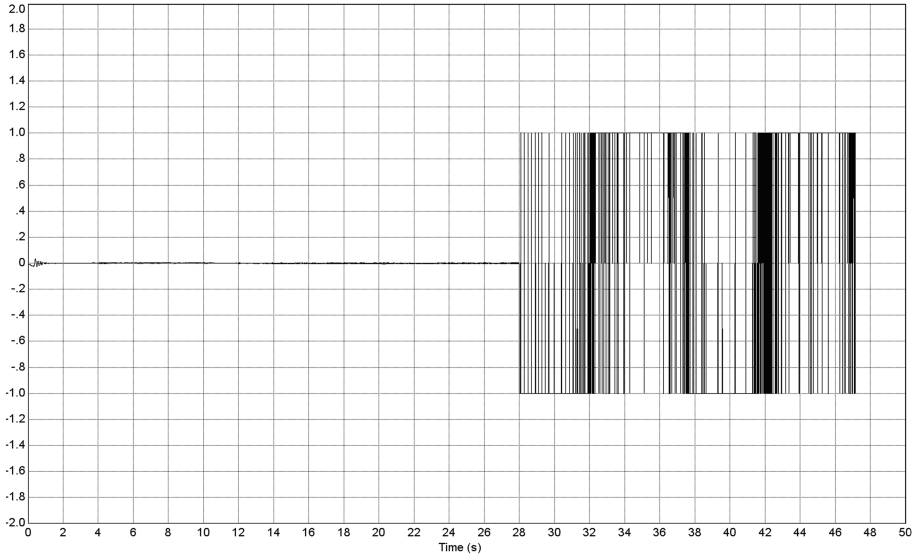

a)

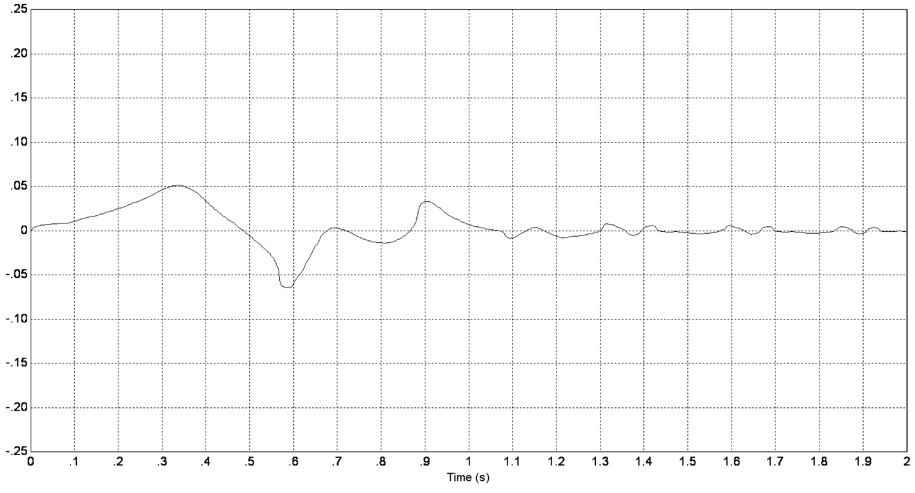

b)

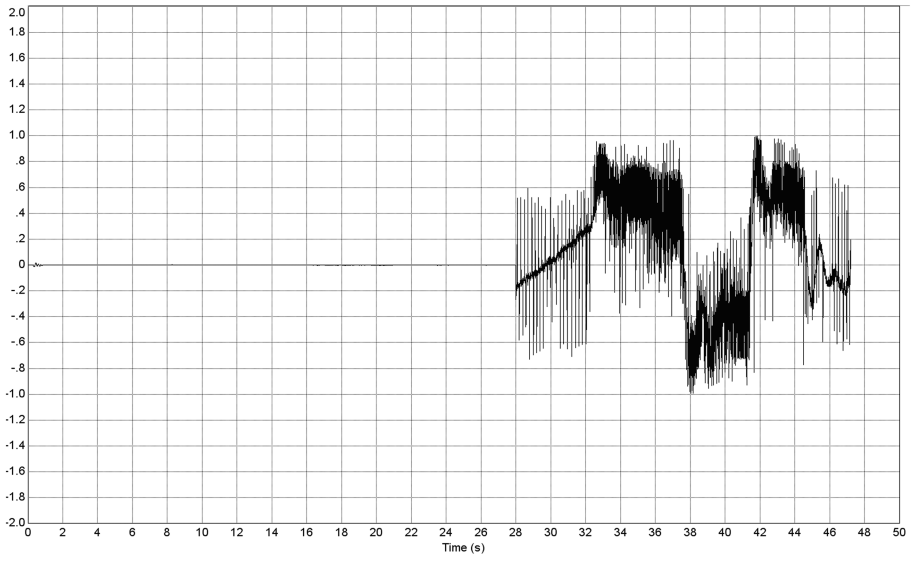

c)

Fig. 15 Illustrations of a) attitude commands, b) attitude commands (zoomed portion), and c) actual (normalized) attitude actuator.

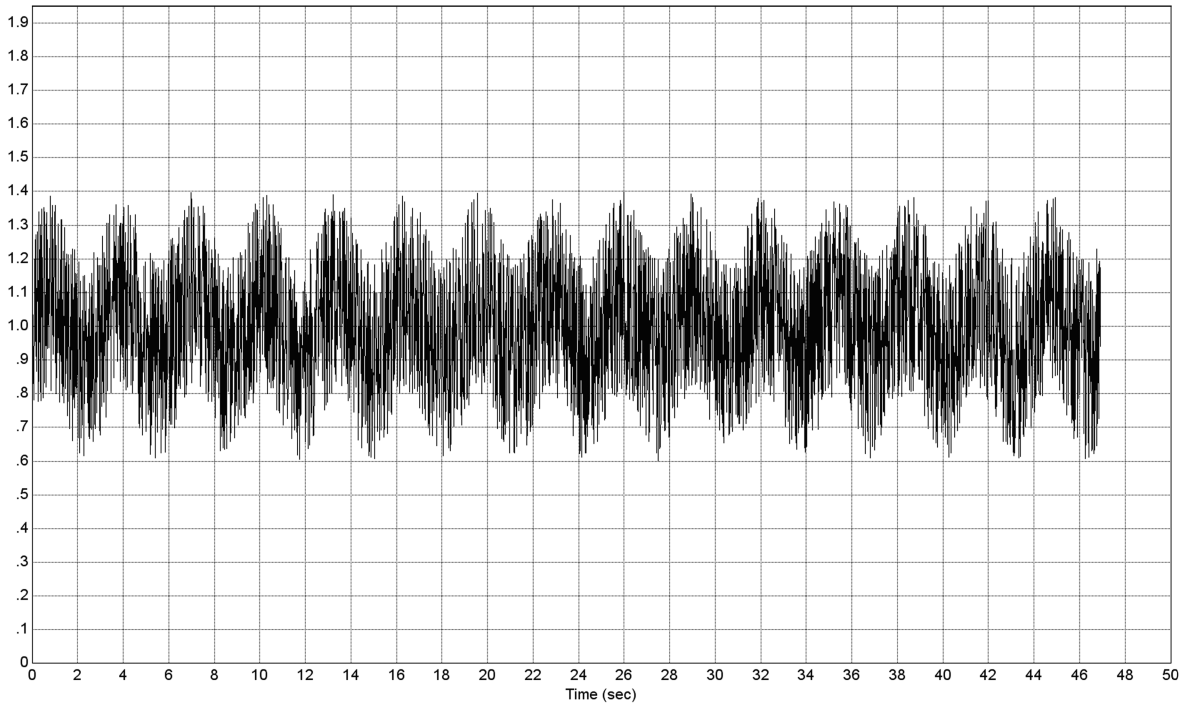

Fig. 16 Typical model disturbance.

the HOSM guidance estimator [Eq. (A3)]. Both estimations are compared with actual target normal acceleration. Figure 12a presents the estimation of the target step maneuver and Fig. 12b shows the estimation of sine-wave maneuvers. Both estimators achieve an amplitude error in the 2–3 m/s range, whereas the estimation lags actual maneuver by less than 0.1 s.

E. Flight-Path Autopilot Performance

The plots in Fig. 13a reveal that the commanded flight-path angle is followed very accurately. One can see the separation between the initial part of the flight, where the interceptor is steered by the continuous angle-of-attack maneuver, with the last part of the flight, where the on–off divert thrusters are used. The ripples in Fig. 13b are the results of the on–off operation of the thrusters.

F. Pitch-Rate Autopilot Performance

Figure 14a shows the tracking of the pitch rate. During the first part of the interception the attitude steering is achieved by continuous TVC control, whereas in the last part it is achieved by the on–off operation of attitude thrusters. Figure 14b represents the tracking of the angle of attack. During the first part of the interception the autopilot accurately tracks the commanded angle of attack. During the second part of the interception the autopilot tracks the pitch rate. Figure 15a represents the composite plot of attitude commands. During the initial part of the interception it represents continuous TVC commands, which are very small in magnitude, whereas in the last portion of the flight it represents commands for the attitude on–off thruster. The TVC deflections represented in the early portion of Fig. 15a are very small, and Fig. 15b represents a zoomed portion of Fig. 15a. Figure 15c represents the corresponding actuator responses. Figure 16 represents a typical multiplicative disturbance plot, with its fast structure driven by the firing of the thrusters and a slow-varying 2–3 s periodical structure.

VI. Conclusions

Novel SSOSM control is used for the missile-interceptor guidance design against a target performing evasive maneuvers. The HOSM estimator reconstructs the target's normal acceleration. The missile autopilot is based on a nonlinear dynamic sliding manifold technique. Integrated SOSM-based guidance–autopilot performance was studied via computer simulations. The excellent results have been obtained against stressing sine-wave target maneuvers. Notwithstanding the rapid pace of the maneuvers, the algorithm achieves extreme estimation and intercept accuracy. Interestingly, the same design allows for seamless operating in the endo- and the exoatmospheric domains. The excellent simulation results were obtained in the presence of very significant model uncertainties, target maneuvers, time delay, and measurement noise.

Appendix: Second-Order Sliding Mode Control

I. Smooth Second-Order Sliding Mode Control

A. *Prescribed Sliding Variable Dynamics*

Consider single-input/single-output (SISO) dynamics of the *first* order:

$$\dot{\sigma} = g(t) + u, \qquad \sigma \in \Re^1 \tag{A1}$$

which is interpreted as the sliding variable [Eq. (14)] dynamics calculated along the system trajectory. The condition $\sigma = 0$ defines the system motion on the sliding surface, $u \in \Re^1$ is a control input that needs to be smooth, and $g(t)$ is a sufficiently smooth uncertain function.

The problem that is addressed in this section is to design *smooth* control u that drives σ and $\dot{\sigma} \to 0$ (smooth second-order sliding mode) in finite time.

The drift term $g(t)$ is to be cancelled by means of a special observer to be developed further. The prescribed compensated σ-dynamics in Eq. (A1) is chosen as

$$\begin{cases} \dot{x}_1 = -\alpha_1 |x_1|^{(p-1)/p} \operatorname{sign}(x_1) + x_2 \\ \dot{x}_2 = -\alpha_2 |x_1|^{(p-2)/p} \operatorname{sign}(x_1), \qquad \sigma = x_1 \end{cases} \tag{A2}$$

Definition: We call a system finite-time stable [22] if it is asymptotically stable with a finite settling time for any solution and initial conditions.

Lemma A1: Let $p \geq 2, \alpha_1,$ and $\alpha_2 > 0$. Then the system in Eq. (A2) is finite-time stable with the settling time being a continuous function of the initial conditions, vanishing at the origin.

See the proof in [15].

B. Nonlinear Disturbance Observer/Differentiator

The sliding variable dynamics in Eq. (A1) are sensitive to the unknown bounded term $g(t)$. Let the variables $\sigma(t)$ and $u(t)$ be available in real time, $g(t)$ be $m-1$ times differentiable, so that $g^{(m-1)}(t)$ has a known Lipshitz constant $L>0$. The control function $u(t)$ is Lebesgue-measurable. Equation (A1) is understood in the Filippov sense [23], which means in particular that $\sigma(t)$ is an absolutely continuous function defined $\forall\, t \geq 0$.

Consider the following observer:

$$\begin{cases} \dot{z}_0 = \nu_0 + u \\ \nu_0 = -\lambda_0 L^{1/(m+1)} |z_0 - \sigma|^{m/(m+1)} \operatorname{sign}(z_0 - \sigma) + z_1 \\ \dot{z}_1 = \nu_1 \\ \nu_1 = -\lambda_1 L^{1/m} |z_1 - \nu_0|^{(m-1)/m} \operatorname{sign}(z_1 - \nu_0) + z_2 \\ \cdots \\ \dot{z}_{m-1} = \nu_{m-1} \\ \nu_{m-1} = -\lambda_{m-1} L^{1/2} |z_{m-1} - \nu_{m-2}|^{1/2} \operatorname{sign}(z_{m-1} - \nu_{m-2}) + z_m \\ \dot{z}_m = -\lambda_m L \operatorname{sign}(z_m - \nu_{m-1}) \end{cases} \tag{A3}$$

Lemma A2: Suppose that $\sigma(t)$ and $u(t)$ are measured with some Lebesgue-measurable noises bounded, respectively, by $\varepsilon > 0$ and $k\varepsilon^{(m-1)/m}$, and $k>0$ is any fixed constant. The parameters λ_i being chosen sufficiently large in the reverse order, the following inequalities are established in finite time for some positive constants μ_i, and η_i depending exclusively on k and the choice of parameters:

$$\begin{cases} |z_0 - \sigma(t)| \leq \mu_0 \varepsilon \\ \cdots \\ |z_i - g^{(i-1)}(t)| \leq \mu_i \varepsilon^{(m-i+1)/(m+1)}, & i = 1, \ldots, m \\ |\nu_j - g^{(j)}(t)| \leq \eta_j \varepsilon^{(m-j)/(m+1)}, & j = 0, \ldots, m-1 \end{cases} \tag{A4}$$

See the proof in [15].

In particular, in the absence of input noises, the exact equalities are established in a finite time:

$$z_0 = \sigma(t), \qquad z_1 = g(t), \ldots, \qquad z_i = \nu_{i-1} = g^{(i-1)}, \qquad i = 1, \ldots, m \tag{A5}$$

It is worth noting that parameters λ_i can be chosen recursively so that parameters $\lambda_0, \ldots, \lambda_k$, which are valid for $m=k$, can serve (after changing the notation) as $\lambda_1, \ldots, \lambda_{k+1}$ with $m = k+1$, which means that only λ_0 is to be assigned. The simulation-checked set 8, 5, 3, 2, 1.5, 1.1 is sufficient for the observer design with $m \leq 5$ (see [14]).

C. Disturbance Cancellation

Let the sliding variable dynamics be of the form in Eq. (A1), with $g(t)$ being $(m-1)$-smooth with a known Lipshitz constant $L>0$ of $g^{(m-1)}(t)$. The prescribed compensated σ-dynamics in Eq. (2) with $p = m+1$ and $m \geq 1$ is easily be provided using the observer in Eq. (A3) via control u:

$$\begin{cases} u = -z_1 - \alpha_1 |\sigma|^{m/(m+1)} \operatorname{sign}(\sigma) + w \\ \dot{w} = -\alpha_2 |\sigma|^{(m-1)/(m+1)} \operatorname{sign}(\sigma) \end{cases} \tag{A6}$$

When exact measurements are available, z_1 becomes equal to $g(t)$ in a finite time, and the σ-dynamics are described by the finite-time stable system in Eq. (2) thereafter.

Theorem A1: Let $m \geq 1$, α_1, $\alpha_2 > 0$, and $g(t)$ be $m-1$-times differentiable, $g^{(m-1)}(t)$ having a known Lipschitz constant $L>0$. Then the closed-loop system in Eqs. (A1), (A3), and (A6) is finite-time stable. If $\sigma(t)$ is measured with some Lebesgue-measurable noises bounded, respectively, by $\varepsilon \geq 0$ and $k\varepsilon^{(m-1)/m}$, then the inequality $|\sigma| \leq \gamma\varepsilon$ is established in finite time for some positive constant γ depending exclusively on the parameters of the controller and the constant k.

See the proof in [15].

Control in Eq. (A6) can be interpreted as a SSOSM control because, being smooth, it provides a finite-time convergence σ, $\dot{\sigma} \to 0$.

The sliding variable in Eq. (A1) and its derivative could also be stabilized at zero in the presence of the disturbance $g(t)$ with a bounded derivative $\dot{g}(t)$ in a finite time using the supertwisting control law :

$$\begin{cases} u = -\alpha_1 |\sigma|^{1/2} \operatorname{sign}(\sigma) + w \\ \dot{w} = -\alpha_2 \operatorname{sign}(\sigma) \end{cases} \tag{A7}$$

However, the supertwisting control law is not smooth and cannot be used in the outer (guidance) control loop but in the autopilot only.

II. Second-Order Sliding Mode Control Based on Nonlinear Dynamic Sliding Manifold

Consider SISO sliding variable $\sigma \in \Re^1$ dynamics of the *second* order:

$$\ddot{\sigma} = g(t) + u \tag{A8}$$

The condition $\sigma = 0$ defines the system motion on the sliding surface, $u \in \Re^1$ is a control input, and $g(t)$ is an uncertain sufficiently smooth function.

One possible SOSM-based control that provides convergence of σ and $\dot{\sigma} \to 0$ in finite-time in the presence of the disturbance $g(t)$ with bounded second derivative can be designed in a format of prescribed convergence law [14]:

$$u = \tilde{\rho} \operatorname{sign}[\dot{\sigma} + |\sigma|^{1/2} \operatorname{sign}(\sigma)], \qquad \tilde{\rho} > 0 \tag{A9}$$

where $\tilde{\rho} > 0$ is sufficiently large.

To avoid differentiation of σ in Eq. (A9), SOSM control u can be also designed based on the NDSM [9,20,21] as follows:

$$\begin{aligned} u &= -\bar{\rho} \operatorname{sign}(J), \qquad J = \sigma + \chi, \\ \dot{\chi} &= \beta_1 |\sigma|^{1/2} \operatorname{sign}(\sigma) - \beta_2 |J|^{1/2} \operatorname{sign}(J) \end{aligned} \tag{A10}$$

where J is the nonlinear dynamic sliding variable, the coefficients are $\beta_2 > \beta_1 > 0$, and $\bar{\rho} > 0$ is sufficiently large. We will call the surface $J=0$ described by the system in Eq. (A10) the NDSM.

Proposition: The control law n Eq. (A10) provides for the finite-time convergent second-order sliding mode $J = \dot{J} = 0$.

See the proof in [20,21].

As soon as the second-order sliding mode $J = \dot{J} = 0$ is established, the sliding variable second-order dynamics in Eqs. (A8) and (A10) are described by

$$\dot{\sigma} = -\beta_1 |\sigma|^{0.5} \operatorname{sign}(\sigma) \tag{A11}$$

and converge to zero in finite time, which is equal to $2\sqrt{e(t_J)}/\beta_2$, where t_J is the moment when NDSM dynamics in Eqs. (A8) and (A10) reach zero (i.e., $J = \dot{J} = 0$).

It is worth noting that the SOSM/NDSM in Eq. (A10) is a high-frequency switching control law. It can be used to generate commands to the on–off thrusters. To achieve a given frequency of control switching, NDSM J can be mixed with a dither signal of a given frequency. In this case the control function in Eq. (A10) will be pulse-width modulated.

III. Continuous Second-Order Sliding Mode (Supertwisting) Control

Again, consider SISO sliding variable $\sigma \in \Re^1$ dynamics of the *second* order given by Eq. (A8). The problem is to design continuous control $u \in \Re^1$ that drives the sliding variable and its derivative to zero in the presence of the bounded disturbance uncertain sufficiently smooth function $g(t)$. To use the continuous supertwisting control in Eq. (A7) we have to reduce the relative degree of the sliding variable dynamics in Eq. (A8) from 2 to 1. To do this an auxiliary sliding variable is introduced:

$$S = \dot{\sigma} + c\sigma, \qquad c > 0 \tag{A12}$$

The coefficient $c > 0$ should be selected to have a given convergence rate $\sigma, \dot{\sigma} \to 0$ in the auxiliary sliding mode $S = 0$. The S-dynamics are derived:

$$\dot{S} = \bar{g}(\sigma, t) + u, \qquad \bar{g}(\sigma, t) = g(t) + c\dot{\sigma} \tag{A13}$$

Assuming that $|\dot{\bar{g}}(\sigma, t)| \le \tilde{L}$, the continuous second-order (supertwisting) control law:

$$\begin{cases} u = -\alpha_1 |S|^{1/2} \operatorname{sign}(S) + w \\ \dot{w} = -\alpha_2 \operatorname{sign}(S) \end{cases} \tag{A14}$$

drives the sliding variable S and its derivative to zero in finite time in the presence of bounded disturbance $\dot{\bar{g}}(\sigma, t)$, although the control gains are to be selected [14,18] $\alpha_1 = 1.5\sqrt{\tilde{L}}$, $\alpha_2 = 1.1\tilde{L}$.

Eventually, $\sigma, \dot{\sigma} \to 0$ as time increases in the auxiliary sliding mode $S = \dot{\sigma} + c\sigma = 0$. Continuous SOSM supertwisting control in Eq. (A7) can be used for generating TVC commands.

References

[1] Kennedy, W. B., and Mikkelsen, C., "AIT Real Gas Divert Jet Interactions; Summary of Technology," *AIAA Defense and Civil Space Programs Conference and Exhibit*, AIAA, Reston, VA, 1998, pp. 225–234; also AIAA Paper 98-5188.

[2] Tournes, C., Shtessel, Y., and Shkolnikov, I., "Autopilot for Missiles Steered by Aerodynamic Lift and Divert Thrusters Using Nonlinear Dynamic Sliding Manifolds," *Journal of Guidance, Control, and Dynamics*, Vol. 29, No. 3, May–June 2006, pp. 617–625. doi:10.2514/1.15486

[3] Zarchan, P., "Tactical and Strategic Missile Guidance," *Progress in Astronautics and Aeronautics*, Vol. 176, AIAA, Reston, VA, 1998.

[4] Chen, W. H., "Nonlinear Disturbance Observer Enhanced Dynamic Inversion Control of Missiles," *Journal of Guidance, Control, and Dynamics*, Vol. 26, No. 1, 2003, pp. 161–166.

[5] Garnell, P., and East, D., "Guided Weapon Control Systems," Pergamon, Oxford, 1977.

[6] Edwards, C., and Spurgeon, S., *Sliding Mode Control: Theory and Applications*, Taylor and Francis, London, 1998.

[7] Idan, M., and Shima, T., "Integrated Sliding Mode Autopilot-Guidance for Dual Control Missiles," *Journal of Guidance, Control, and Dynamics*, Vol. 30, No. 4, 2007, pp. 1081–1089. doi:10.2514/1.24953

[8] Moon, J., Kim, K., and Kim, Y., "Design of Missile Guidance Law Via Variable Structure Control," *Journal of Guidance, Control, and Dynamics*, Vol. 24, No. 4, 2001, pp. 659–664.

[9] Shkolnikov, I., Shtessel, Y., and Lianos, D., "Integrated Guidance-Control System of a Homing Interceptor: Sliding Mode Approach," 2001 AIAA Guidance, Navigation, and Control Conference, AIAA Paper 2001-4218, 2001.

[10] Thukral, A., and Innocenti, M., "Sliding Mode Missile Pitch Autopilot Synthesis for High Angle of Attack Maneuvering," *IEEE Transactions on Control Systems Technology*, Vol. 6, No. 3, 1998, pp. 359–371. doi:10.1109/87.668037

[11] Babu, K., Sarma, I., and Swamy, K., "Switched Bias Proportional Navigation for Homing Guidance Against Highly Maneuvering Target," *Journal of Guidance, Control, and Dynamics*, Vol. 17, No. 6, 1994, pp. 1357–1363. doi:10.2514/3.21356

[12] Zhou, D., Mu, C., and Xu, W., "Adaptive Sliding-Mode Guidance of a Homing Missile," *Journal of Guidance, Control, and Dynamics*, Vol. 22, No. 4, 1999, pp. 589–594.

[13] Yeh, F.-K., Chien, H.-H., and Fu, L.-C., "Optimal Midcourse Guidance Sliding-Mode Control for Missiles with TVC," *IEEE Transactions on Aerospace and Electronic Systems*, Vol. 39, No. 3, 2003, pp. 824–837. doi:10.1109/TAES.2003.1238739

[14] Levant, A., "Higher-Order Sliding Modes, Differentiation and Output-Feedback Control," *International Journal of Control*, Vol. 76, Nos. 9–10, 2003, pp. 924–941. doi:10.1080/0020717031000099029

[15] Shtessel, Y., Shkolnikov, I., and Levant, A., "Smooth Second Order Sliding Modes: Missile Guidance Application," *Automatica*, Vol. 43, No. 8, 2007, pp. 1470–1476. doi:10.1016/j.automatica.2007.01.008

[16] Shtessel, Y., Shkolnikov, I., and Brown, M., "An Asymptotic Second-Order Smooth Sliding Mode Control," *Asian Journal of Control*, Vol. 4, No. 5, 2003, pp. 498–504.

[17] Shtessel, Y., Tournes, C., and Shkolnikov, I., "Guidance and Autopilot for Missiles Steered by Aerodynamic Lift and Divert Thrusters Using Second Order Sliding Modes," The Conference on Guidance, Navigation and Control, AIAA Paper 2006-6784, Aug. 2006.

[18] Levant, A., "Sliding Order and Sliding Accuracy in Sliding Mode Control," *International Journal of Control*, Vol. 58, No. 6, 1993, pp. 1247–1263. doi:10.1080/00207179308923053

[19] Wise, K. A., and Broy, D. J., "Agile Missile Dynamics and Control," *Journal of Guidance, Control, and Dynamics*, Vol. 21, No. 3, 1998, pp. 441–449.

[20] Krupp, D., Shkolnikov, I. A., and Shtessel, Y. B., "2-Sliding Mode Control for Nonlinear Plants with Parametric and Dynamic Uncertainties," The Conference on Guidance, Navigation, and Control, AIAA Paper 2000-3965, 2000.

[21] Shkolnikov, I., Shtessel, Y., and Lianos, D., "The Effect of Sliding Mode Observers in the Homing Guidance Loop," *Proceedings of the Institution of Mechanical Engineers, Part G: Journal of Aerospace Engineering*, Vol. 219, No. 2, 2005, pp. 103–111. doi:10.1243/095441005X30199

[22] Bacciotti, A., and Rosier, L., "Lyapunov Functions and Stability in Control Theory," *Lecture Notes in Control and Information Sciences*, Vol. 267, Springer–Verlag, New York, 2001.

[23] Filippov, A. F., *Differential Equations with Discontinuous Right-Hand Side*, Kluwer, Dordrecht, The Netherlands, 1988.